This Thesis committee for Benjamin James List

Certifies that this is the approved version of the following thesis

Development of Self-Heating Pipeline Pigging Tool

APPROVED BY

SUPERVISING COMMITTEE

Mukul Sharma, Supervisor

Paul Bommer, Co-Supervisor

Development of Self-Heating Pipeline Pigging Tool

By

Benjamin James List

Thesis

Presented to the Faculty of the Graduate School

Of The University of Texas at Austin

In Partial Fulfillment

Of the Requirements

For the Degree of

Master of Science in Engineering

The University of Texas at Austin

August, 2017

Acknowledgments

"It takes a village to raise a child."

I cannot take all, or even most, of the credit for the success of this project. As such, I'd like to acknowledge a few villagers who helped in the upbringing this thesis.

Dr. Sharma, at a certain point in many professors careers they gain the sense of infallibility. They have convinced themselves that they have seen it all and understand exactly what is going on. Despite your tremendous success and notoriety, you have maintained an almost child-like eagerness to gain new understanding through the research being done in your group. It is remarkable that you can maintain this enthusiasm for the work of each of your students. I don't know how you do it. I would like to thank you for your support and interest in my work. I can say that this project has been a pleasure and has helped me grow as a person. Thank you for this wonderful opportunity.

Rod, I should have listened to everything you said you from day one. If I had, I would have finished this thesis at least six months ago. During our weekly meetings, you never backed down from what you thought was right even if it was not popular. Looking back now, you were mostly right. And in a department full of eggheads who could only understand equations, you brought practicality and can-do ingenuity to the laboratory. When I needed to design a part for testing, I would just have to tell you how I found the device in a catalog and how much that device would cost. The MacGyver wheels in your head would start turning, and soon enough we would have a better solution ready that day. Spending time with you has taught me to have confidence in my own ingenuity.

Jin, during my graduate school orientation Professor Mohanty remarked to the assembly "See that lady there (Franky). She is my boss. While assistants may not have the title, they are the ones running the place." After joining Dr. Sharma's group, I found that certainly was the case. You somehow managed to keep this group of over twenty afloat. If I needed parts the next day for my project, recommendations on who to talk to about a problem, or a little afternoon pick-me-up snack and coffee, there was one person I could always come to. I'd like to thank you for doing a largely thankless job.

Daryl, I cannot begin to remember all the times I knocked on your door outside of the clearly posted student hours and how many times you opened that door. Decades of experience as a machinist have taught you how to build and design instrumentation. Decades of experience I did not have and needed to finish this project. I relied on your machinist experience and your facilities countless times. I would like to thank you for always keeping your doors open for me.

Development of Self-Heating Pipeline Pigging Tool

by

Benjamin James List, MSE

The University of Texas at Austin, 2017

Supervisor: Mukul Sharma

Paraffin deposition has been a long standing problem in pipeline flow assurance. The cooling of oil during transit in pipelines results in the deposition of paraffin onto pipeline walls. These depositions can lead to decreased throughput of the pipeline and decrease crack detection of smart pigs. Traditional methods of handling paraffin deposition include pushing wax down the line with pigging tools and solubilizing wax with heated oil. This paper investigates a novel method to address this issue: a self-heating pipeline pigging tool. This design utilizes a set of turbines driven by a by-pass flow through the pig. The turbines turn an inductive heating magnet array which heats the pig to reintroduce wax into the oil as the pig pushes the wax down the pipeline. The thesis work enclosed in this paper shows how we successfully designed and built a laboratory scale heater component of the pigging device. The turbine and inductive heating array were designed, built, and tested separately before coupled together. Efficiencies of 78% were achieved in the laboratory testing. Further work needs to be done to scale the heater to field scale and implement the heater into a working pigging device.

Table of Contents

Table of Contents iii
Table of Tables v
Table of Figures vi
Chapter 1. Introduction 1
Chapter 2. Background 3
Pigging 3
Types of Pigs 3
Paraffin Buildup 5
Inductive Heating 5
Halbach Arrays 8
Turbines 11
Types of Turbines 11
Specific Speed 13
Euler's Equation of Turbomechanics 14
Radial Equilibrium Theory 16
Chapter 3. Methodology 18
Overview of Experiments 18
Magnet Testing 19
Turbine Testing 20
Coupled Testing 22
Modeling and Verification of Magnet Performance 25
Modeling using Ansys 25
Experimental Verification 27
Design of Turbines and Performance Evaluation under Pigging Constraints 30

Performance Driven Turbine Design 30
Performance Evaluation Under Pigging Conditions 40
Overall Energy Balance of EM-Pig in Operation 57
Chapter 4. Results and Discussion 60
Halbach Performance 60
Ansys Simulation Results 60
Experimental Results 61
Comparison 62
Turbine Performance 63
Effect of Specific Speed on Performance and Efficiency 63
Performance Curves under Varying Speed and Flow Rate 66
Chapter 5. Conclusions 73
Chapter 6. Appendix 74
Appendix A- Methodology 74
Appendix B- Halbach 75
Appendix C- Turbine Tests 77
References 79

List of Tables

Table 1 Magnetic strength of differing magnetic arrays (Duramag, 2015) 9
Table 2 Recommended operating range for varying turbines (White, 2016)..... 14
Table 3 Halbach Ansys test matrix with base values bolded 26
Table 4 Power regression results of Ansys simulation 61
Table 5 Performance Benchmarks of Varying Specific Speed Turbines..... 65
Table 6 Efficiencies without Orifice Effect 66
Table 7 Ansys Simulation with varying pipe diameter and speed 75
Table 8 Ansys Simulation with varying air gap, pipe wall thickness, and pipe wall material 75

List of Figures

Figure 1. Pipeline before and after spear. 4
Figure 2. Eddy currents induced in a moving conductive disc (Courtin et al., 2016). 7
Figure 3. Halbach pattern where the arrow indicates the north seeking side of the magnet. 9
Figure 4. Circular Halbach array with field lines (left)..... 10
Figure 5. Circular Halbach array with equipotential field lines (Merritt et al., 1994) (right)..... 10
Figure 6. . Pelton Wheel (White, 2016). 12
Figure 7. Axial Turbine. 12
Figure 8 Radial Turbine. 12
Figure 9. Expected efficiencies for turbines at varying ns (White, 2016)..... 13
Figure 10. Diagram of fluid flow through turbine. 15
Figure 11. Inlet and outlet triangles of a turbine. 16
Figure 12. Convection occurring from radial forces. 17
Figure 13. Testing Methodology Flow Chart. 19
Figure 14. Halbach Performance Curve. 20
Figure 15. Variable Flow Rate Performance Curves. 22
Figure 16. Overlaid Halbach/turbine performance. 23
Figure 17. Overlay with gear ratio. 24
Figure 18. Overlay with highlighted intersections. 24
Figure 19. Halbach Ansys Model. 26
Figure 20. Halbach Heating Test Set-Up. 28
Figure 21. Halbach array used in Halbach and coupled testing. 28
Figure 22. Stator/Rotor Diagram with Blade Angles (Turton, 1995). 34
Figure 23. Outlet velocity triangle. 34
Figure 24. Inlet velocity triangle. 35
Figure 25. Example Calculation of Short Blade Turbine. 36
Figure 26. Blade Being Extruded From Single Shape. 37
Figure 27. Long Blade being Lofted. 38
Figure 28. Lofted Long Blade Turbine (Right). 39
Figure 29. Extruded Short Blade Turbine. 39
Figure 30. 3D Rendering of turbine stator on 3D printing program. 40
Figure 31. Test Bed Schematic. 41
Figure 32. Dwyer Pressure Gauge. (Dwyer Instruments, 2017.) 43
Figure 33. Turbine Housing Endcaps. 45
Figure 34. Flow Distribution with Diffuser Plate. 46
Figure 35. Types of Misalignment. 47
Figure 36. Diagram of misalignment from uneven ends. 47
Figure 37. Braking wheel. 49
Figure 38. CAD Drawing of EM-Heater without the aluminum pipe. 51
Figure 39. Turbine test bed. 52

Figure 40. 80 n_s turbine.....55
Figure 41. 140 n_s turbine.....55
Figure 42. 40 n_s turbine.....56
Figure 43. Maximum wax dissolved by pig. 59
Figure 44. Halbach array heating results. 62
Figure 45. Turbine Performance Curves at Varying Specific Speeds. 64
Figure 46 Performance Curves at Varying Flow Rates.....67
Figure 47 Torque Curves of Various Turbines.....68
Figure 48. Magnet and Turbine Pairing for 68GPM. 69
Figure 49. Magnet/Turbine Performance For Varying Flow Rates. 70
Figure 50. Predicted and Observed Coupled Turbine/Magnet Performance. 71
Figure 51. Screenshot of Blade Geometry Spreadsheet. 74
Figure 52. Power regression of speed sensitivity test. 76
Figure 53. Power regression of diameter sensitivity test. 76
Figure 54. Maximum Power with Varying Flow Rates. 77
Figure 55. Max Power Observed Relationship to Speed in N_{sp} 140 Turbine. 78

Chapter 1. Introduction

The flow of oil can lead to the buildup of various substances on the pipeline wall. These substances have been known to erode, corrode, and plug up pipelines. The deposition of paraffin wax is of primary concern to operators and pipeline service companies (Gupta, 2015). Not only does paraffin impede flow, but it also prevents diagnostic tools from gauging pipeline health (US DOT, 2014).

Paraffin Deposition occurs when an oil containing wax encounters temperature, pressures, and flow conditions which are favorable for wax precipitation. This could occur anywhere from the near wellbore region all the way to the holding tanks at the refineries. The greatest factor in wax precipitation is the effect of temperature (Todi et al., 2006). Cold pipelines such as the Alyeska pipe and subsea pipelines are especially susceptible to paraffin deposition.

Pipeline service companies currently employ pigging tools to remove this deposition. “Pigs” are mechanical plugs that are driven down the pipeline by the differential pressure across them. They remove wax and other debris by scraping the pipe walls as the travel with the oil. There are many pig varieties, each with their own niche and design features. All pigs achieve the same goal: they push the wax out.

Pigging pipelines this way can lead to serious problems when deposits of paraffin are harder or are larger than expected (Fung et al., 2006). There have been many cases where pigs have encountered these difficult deposits and required high differential pressures to force the pig down the pipeline. Dissolving the wax by reheating could put the wax back into solution and would eliminate these scenarios where there is too much wax for the pig to handle. If too much wax accumulates and the pressure required to push the pig along become too high, the pig is then stuck and will require intervention.

Remedial techniques for stuck pigs include hot tapping in conjunction with paraffin inhibitors, or hot oil and the use of a rescue pig (Al-Yaari, 2011). All of these solutions have an associated lag time until they are effective, and they require an operator(s) and materials on

site. If these solutions fail to free the pig, the pipeline may need to be shut down temporarily to cut out the stuck pig.

Heating oil has been and is done to mitigate wax deposition. The Alyeska Pipeline operators have had to install several heaters at pump stations to combat wax deposition (Bailey, 2016). The hot tapping and injection of hot oil for stuck pigs uses hot oil to dissolve wax. Both of these require modifications to the pipelines and heat the entirety of the oil. Locally heating the wax to dissolve it into the oil with a self-heating pig, is less energy intensive and does not require retrofitting of the existing pipelines. The aim of this project is to develop a pig that could heat its self to dissolve the wax ahead of it.

The pressure potential across the pig can be harnessed through the application of turbines. Similar to the method applied in hydroelectric dams, a set of turbines can generate power using the flow of oil through the pig. Where dams generate electricity, the self-heating pig generates heat. Not requiring electricity allows the use of inductive heaters, which operate similar to generators but only produce heat. This paper describes the investigative process of designing and testing this turbine/inductive heater for use in a self-heating pig.

Chapter 2. Background

Developing a self-heating pigging tool required knowledge of the current pigging tools, inductive heating, and the turbines that power the inductive heater. This section provides the background and theory needed for these three topics.

Pigging

The rumor is that pigging gets its name from the sound it makes as it travels down the pipeline. The contact between the pig and pipeline makes a sound similar to the squealing of a pig. This tight fit allows for the pigs to scrape off any potentially corrosive residue on the pipe walls. This section describes the different types of pigging tools along with the residue that often accumulates in the pipeline.

Types of Pigs

The pigs in use today can fall into one of two distinct categories smart and clean pigs. Cleaning pigs clean the pipelines from debris such as paraffin, rust, or scale. Smart pigs inspect the pipeline for weak points that could lead to failure.

Cleaning Pigs

Cleaning pigs remove paraffin deposition from the pipeline walls through mechanical shearing. Paraffin deposition can increase pressure losses through the pipe and hinder the cleaning pig implementation. Typically, cleaning pigs are run on a regular cleaning schedule to keep the deposition at a minimum. Cleaning pigs are used before an inspection pigs as the tools on the smart pigs require clean pipe walls. The industry has designed cleaning pigs in a variety of shapes and size depending on the particular application.

There are three broad categories of cleaning pigs: Mandrel, Foam, and Spherical. Mandrel pigs have a steel center tube with larger diameter components attached to the mandrel. Foam pigs are soft-bodied pigs often made from polyurethane. Foam pigs' soft bodies have the advantage over mandrel pigs of being able to navigate tight turns and pass over deformities in the pipeline. Spherical Pigs are either of solid construction or are inflatable. Their spherical body allows for navigation of any bend. They do not remove deposition well, and are only used on pipelines where other pigs cannot go. (Hashem, 2016)

Spears

Spears are a subset of cleaning pigs.

Between the well head and the storage tanks, wax can build up especially in waxy crudes. The wax can dislodge from the pipe wall leading to an obstruction to flow down the pipe. The obstruction could then lead to a higher pressure loss over the pipe and decreased production from the well. The increased pressure loss is an area of concern for operators.

If a well is expected to have wax problems, spears might be considered to mitigate the issue. Spears are an under-gauge pigs that can remove these obstructions, see Figure 1. By keeping the pig under-gauge, there is little risk of a stuck pig as there is room for the pig to navigate around an indentation in the pipe wall. The smaller diameter of the pig means that the spear leaves behind a considerable layer of wax.

The spears are typically fed into the pipe and retrieved using an automated system. They are usually run several times a week to ensure high production from the well.

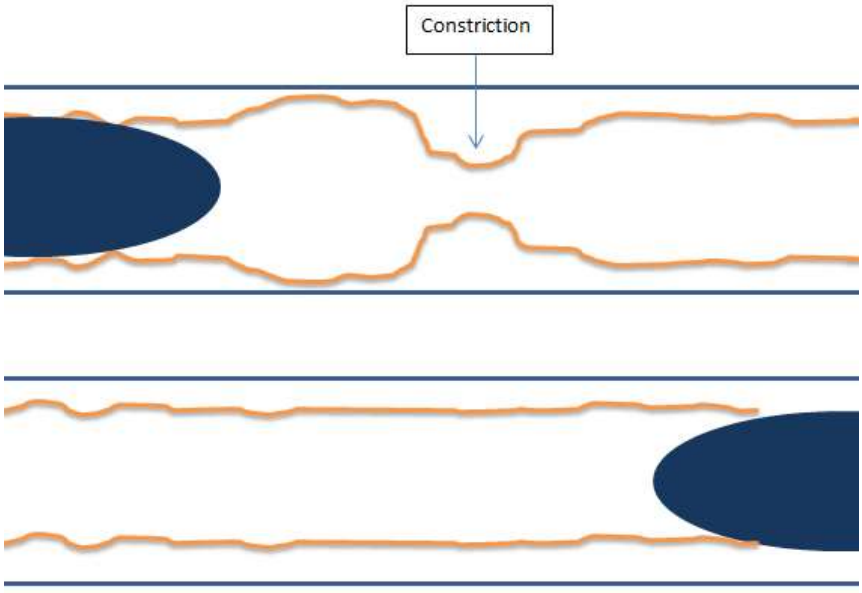

Figure 1. Pipeline before and after spear.

Smart Pigs

Smart pigs are the newest addition to the fleet of pigging tools. Smart pigs do not clean the pipeline, unlike the other two types mentioned. Their purpose is to gather information on

the pipeline such as; pipeline diameter, curvature, pipe wall thickness, flaws in the pipe that could cause leakage, and corrosion. They are equipped with an array of tools and sensors that allow them to assess the pipeline condition (SCGC, 2013).

Two of the most common tools are Magnetic Flux Leakage (MFL) and Ultrasonic (US). MFL tools induce a magnetic flux in the pipeline wall and use sensors to measure the flux leak off. The flux leakage can be used to detect defects in the pipeline wall. Ultrasonic tools emit a high-frequency sound wave and measure the response to assess wall thickness and flaws in a process similar to that used for prenatal imaging (US DOT, 2014). Between these two tools, operators can determine the condition of the pipeline.

Pipeline inspection is critical to identifying corrosion and implementing preventative maintenance. Increasing regulation has mandated that pipeline companies regularly monitor pipeline health through smart pigs. This new set of laws, in turn, requires companies to regularly clean their pipes as paraffin deposition can prevent smart pigs from detecting flaws (Waldman, 2016).

Paraffin Buildup

Paraffin is a component of many crude oils, ranging from C_{20} to C_{80} molecules (Dobbs, 1999). Paraffin is regarded as inert as it is comprised mainly of alkanes. While they do not react in the pipeline, they still cause headaches for pipeline operators and service companies.

Paraffin has limited solubility in most crudes, and this solubility only decreases as the oil cools. Paraffin is known to deposit throughout the production chain from the wellbore to the pipelines, separators, and holding tanks (Seredyuk et al., 2009). Paraffin deposition reduces the effective diameter of the pipeline and increases the surface roughness of the pipeline (Wit, 2015). Furthermore, paraffin deposition can inhibit tools from monitoring the pipeline health (Waldman, 2016). Paraffin mitigation is estimated to cost the industry hundreds of millions of dollars each year (Bagdat et al., 2015).

Inductive Heating

Inductive heating is the process of heating an electrically conductive material as changing magnetic fields induce currents in the material, which then is heated through resistive

heating. To understand inductive heating a general understanding of electromagnetism is essential.

Faraday's Law of Induction states that:

> The induced electromotive force (Induced Voltage) in any closed circuit is equal to the negative of the time rate of change of the magnetic flux enclosed by the circuit.

(Jordan et al., 1968)

Or in a mathematical form:

$$\varepsilon = -\frac{d\Phi_B}{dt} \quad \textbf{[1]}$$

Where:

ε is the electromotive force (Volts)

Φ is the magnetic flux (Wb or Volts*s)

t is time (seconds)

The change in the magnetic flux, in equation 1, can be time-dependent variations in the local field, such as in alternating current electricity where the alternating current alternates the magnetic field in a nearby conductor. This time-dependent change in flux is what is responsible for a large source of losses in transformers and AC motors (Haimbaugh, 2001). The change in magnetic flux can also be a result of the magnetic field moving about the workpiece, see Figure 2. The lines in green are the magnetic field lines, and the lines in red are the induced eddy currents.

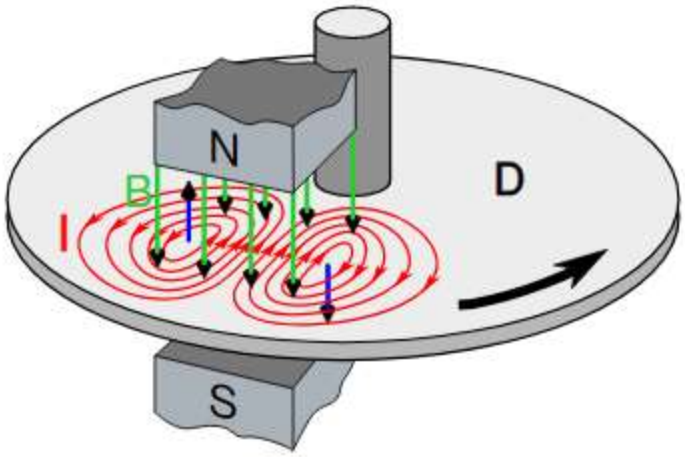

Figure 2. Eddy currents induced in a moving conductive disc (Courtin et al., 2016).

Eddy currents get their name from the circular motion which resembles eddies observed in fluids. Using the left-hand rule, the current in the piece is in the direction into the page. These eddy currents moving through the material produce heat from resistive heating. Resistive heating is responsible for the heating in toasters and the warmth incandescent light bulbs give off. Assuming there is full penetration of the magnetic field through the metal, the heat dissipation from eddy currents in Figure 2 can be expressed as (Courtin et al., 2016)

$$P = \frac{\pi^2 B_p d^2 f^2}{6k\rho D}$$

[2]

Where:

P is the heat dissipation per unit mass of work (W/kg)

B_p is the peak magnetic field strength (T)

d is the thickness of the work

f is the frequency (Hz)

k is a constant, in this case, 1

ρ is the resistivity of the material (Ω*m)

D is the density of the material (kg/m^3)

The left-hand rule also shows that there is a force doing the work, in Figure 2, in the clockwise direction. The induced force will experience a drag as it rotates through the magnetic field. The torque required to rotate the object can be solved from an overall energy balance as the work done in spinning the object will be equal to the heat dissipated.

Using a slightly modified version of [2, the power (P) and the torque can be expressed as:

$$P = \omega * \tau = \frac{\pi^2 B_p d^2 \omega^2 m}{6k\rho D} \quad [3]$$

$$\tau = \frac{\pi^2 B_p d^2 \omega m}{6k\rho D} \quad [4]$$

Where:

τ is torque (N*m)

ω is angular velocity (rad/s)

This relationship between the power or torque required to spin the conductor in the magnetic field is useful later when calculating the power requirements for the turbine to rotate the magnetic array.

Halbach Arrays

All magnetic arrays are not created equal. Some perform better than others.

The magnetic patterns used in Halbach arrays were first proposed in 1973 by a John Mallinson and later were independently discovered by Klaus Halbach, for whom the arrays are named . The Halbach array is a four magnet sequence, as seen in Figure 3. The Halbach arrays have the ability to increase the total field strength over other arrays, see Table 1.

Figure 3. Halbach pattern where the arrow indicates the north seeking side of the magnet.

Table 1. Magnetic strength of differing magnetic arrays (Duramag, 2015).

Three Magnet Geometries Inspected Through Three Different Operational Gaps			
	Attractive Force (lbf.)		
Gap (Inch)	All NORTH	Alternating N-S-N-S-N	Halbach Array
0.000"	80	105	112
0.010"	70	91	102
0.060"	36	36	57

The Halbach array has the effect of creating lobes of high magnetic field intensity, as seen in Figure 5 and **Figure 6**. When the Halbach array is constructed circularly, these nodes give the impression of a flower with petals. The peak of the petals, or nodes, has the highest field strength, and between the petals, the field strength drops. If a metal cylinder is placed outside of the array, as depicted in Figure 5, the alternating of high and weak field strength generates large changes in the magnetic flux when the array is spun. The ability for the Halbach array to produce substantial changes in magnetic flux makes it an attractive option for inductive heating.

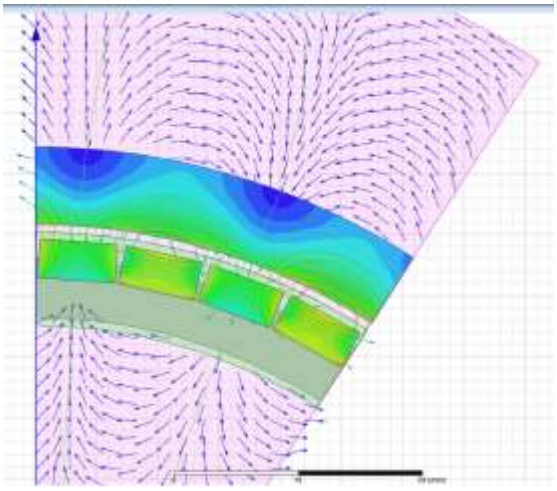

Figure 4. Circular Halbach array with field lines (left).

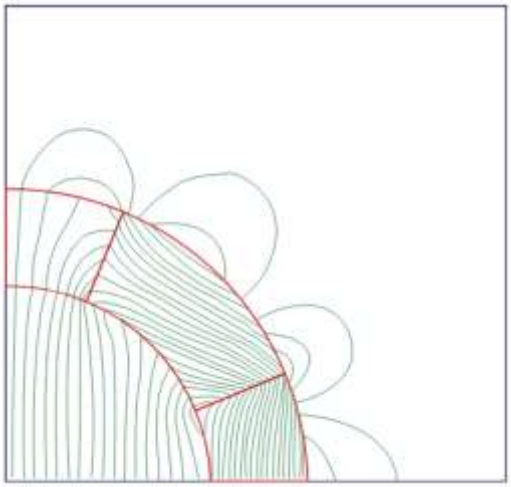

Figure 5. Circular Halbach array with equipotential field lines (Merritt et al., 1994) (right).

While the Halbach arrays provide excellent performance for inductive heating applications, there are a few considerations that should not be neglected. The magnets of the Halbach array are not in their preferred orientation, so they push against each other. (Duramag, 2015) When using strong magnets, this pushing can make assembly difficult and requires attention to the method of securing the magnets. Second, magnets have a tendency to lose their magnetic strength while at higher temperatures. For the high performing neodymium magnets, this temperature is around 80-100^{o}C. (K&J Magnets, 2014) If operated above those temperatures, the magnets will lose field strength even after they are cooled. This may pose challenges to keep the magnets cool while using them in a heater.

Turbines

Turbines are devices which extract energy from a moving fluid and convert that energy into useful work. Most people think of wind farms or jet engines when they hear the word turbines. Turbines are also widely used in power generation for hydroelectric generation. This class of turbine which works with incompressible fluids has a different design than the turbines that work with compressible fluids. This section entails the background and theory needed to understand how these turbines operate.

Types of Turbines

There are many distinct designs of the turbine, and each type has its strengths and operational niches. There are three major classifications of turbines; Pelton Wheels, Axial, and Radial. In a Pelton wheel or impulse turbine, the working fluid is jetted through a nozzle into a bucket where the momentum change imparts a force on the wheel driving it forward. A picture of a Pelton wheel can be seen in Figure 8. Pelton wheels work most efficiently in high torque and low angular speed conditions. Axial turbines are similar in design to propellers. In an axial turbine, the working fluid travels in the same direction as the axis of rotation of the turbine, see **Figure 6**. These turbines perform most efficiently at high speed and low torque conditions. Radial turbines, or Francis turbines, are turbines where the working fluid enters perpendicular to the axis of rotation, see **Figure 7**. These turbines perform in the area between Pelton wheels and axial turbines.

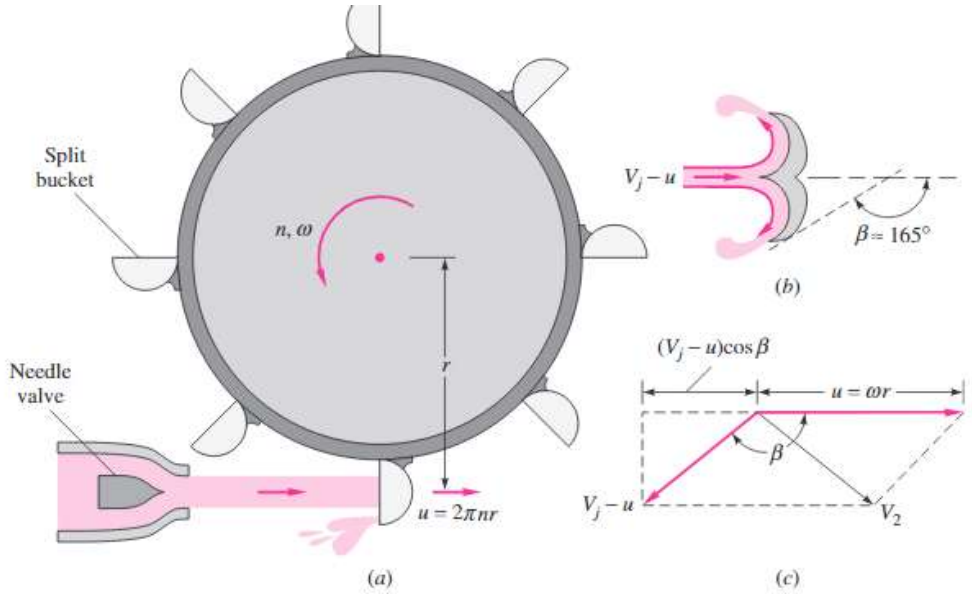

Figure 6. . Pelton Wheel (White, 2016).

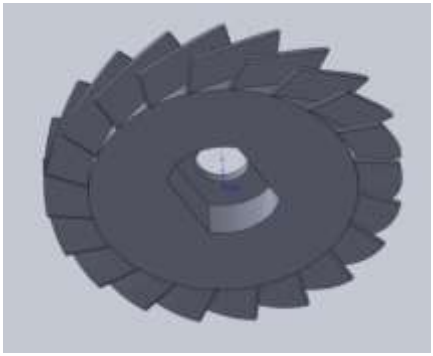

Figure 7. Axial Turbine.

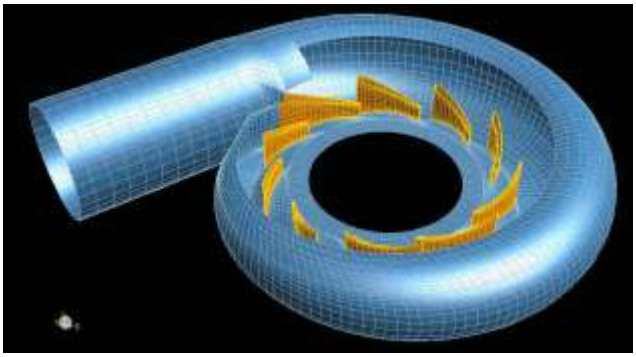

Figure 8 Radial Turbine.

Specific Speed

The specific speed is the revolutions per minute required to produce 1kW of power while operating with 1 meter of head. The equation for specific speed is:

$$n_s = \frac{n * \sqrt{P}}{H^{\frac{5}{4}}}$$

[5]

Where n is RPM, P is in kW, and H is in meters of head.

A turbine with a low specific speed can produce the same amount of power at lower RPMs. The lower the specific speed, the higher the torque and the lower the operating speed. Each turbine type performs best under certain specific speeds, See Figure 9.

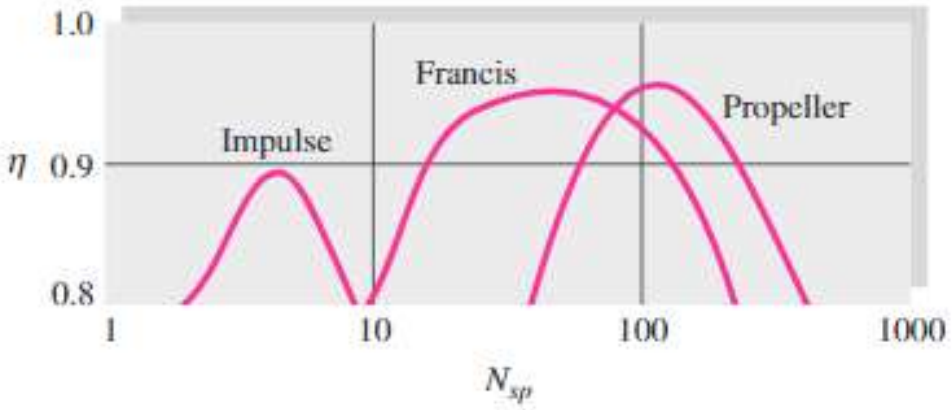

Figure 9. Expected efficiencies for turbines at varying n_s (White, 2016).

Table 2. Recommended operating range for varying turbines (White, 2016).

Turbine type	N_{sp} range	C_H range
Impulse	1–10	15–50
Francis	10–110	5–25
Propeller:		
Water	100–250	1–4
Gas, steam	25–300	10–80

Choosing the right turbine for the n_s conditions is important to maximize the efficiency of the turbine.

Euler's Equation of Turbomechanics

In the turbine, the force acting on the blades can be found from the change in momentum of the working fluid, and the distance is the distance traveled by the spinning rotor. We can express this force as:

$$F = \frac{\Delta momentum}{time} \quad [6]$$

Where $\Delta momentum = \Delta velocity * mass$

So,

$$F = \Delta v * \dot{m} \quad [7]$$

And

$$\tau = (\Delta v * \dot{m}) * r \quad [8]$$

This, equation 8, is Euler's Equation of Turbomachinery.

In a pipe flow of an incompressible fluid such as oil or water, the velocity down the pipe cannot be changed without a constriction and the radial velocity will always be 0. This leaves the rotational velocity (V_θ)as the velocity component from which the turbine will derive its power.

To manipulate V_θ, rotors and stators are used. The rotors are the rotating piece that extracts the energy from the working fluid. The stators remain stationary and prime the working fluid by giving it the required whirl, a V_u component, which the rotor can manipulate to generate force and power.

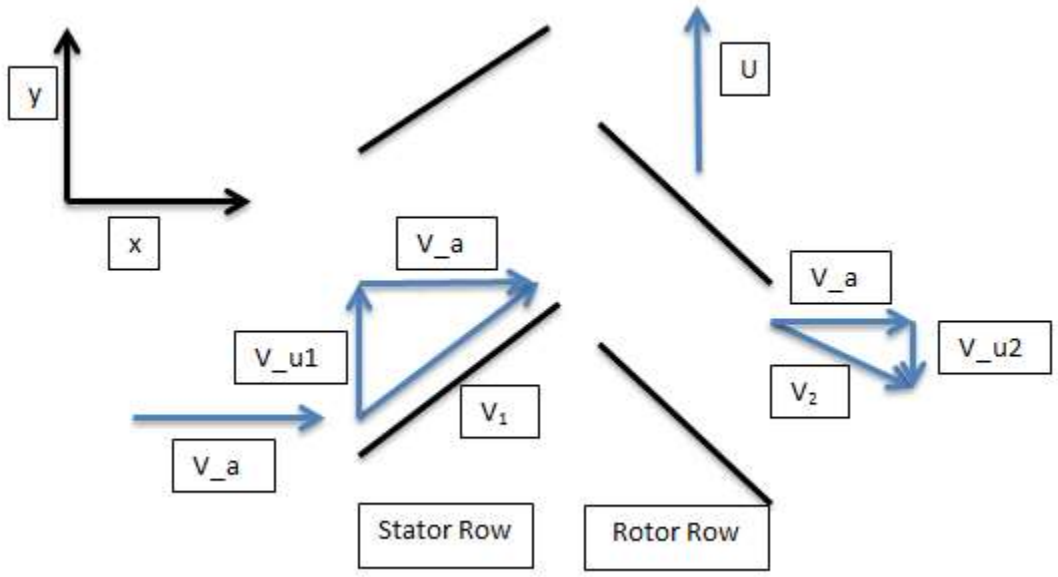

Figure 10. Diagram of fluid flow through turbine.

To help illustrate how the rotors and stators manage the radial velocity (V_θ), refer to Figure 10. The working fluid enters the stator with a velocity V_a and leaves the stator at the same angle as the stator with a V_u component. The working fluid then enters the rotor and, its radial velocity is altered by the rotor, resulting in a change in radial velocity. This ΔV_u, as seen in Figure 11, results in a force on the rotor. Since the working fluid is applying a force on the rotor over a distance, as the rotor spins, the result is work being done on the rotor. This is how a turbine generates power. The method which the blade angles can be used to generate a target power is described in the *Methodology* section.

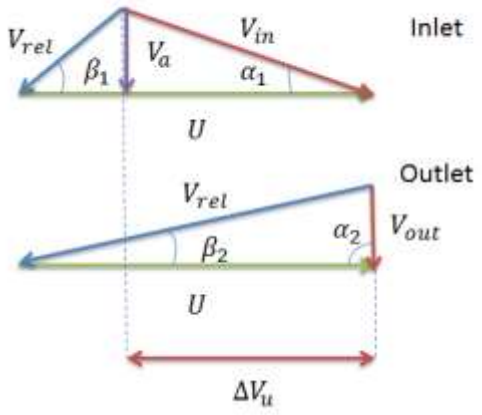

Figure 11. Inlet and outlet triangles of a turbine.

Radial Equilibrium Theory

In an axial turbine, if V_u is constant radially, there is a pressure gradient towards the tip due to the centrifugal forces acting on the fluid. As the fluid speeds up through the stator, there is a pressure drop from the venturi effect. This applies an opposing pressure gradient to the centrifugal forces. These two forces are at equilibrium when the velocity profile is (Turton, 1995):

$$V_u = r^{-1} * constant \quad [9]$$

Where:

V_u is the velocity in the u direction or the θ component of velocity in radial coordinates (m/s)

r is radius or the distance on the blade from the axis of rotation (m)

When the forces are not in equilibrium, when equation [9] does not hold true, there will be a pressure gradient radially. This can cause convection cells to form between the rotor blades. This will result in a loss of efficiency and introduce modes of vibration in the blade.

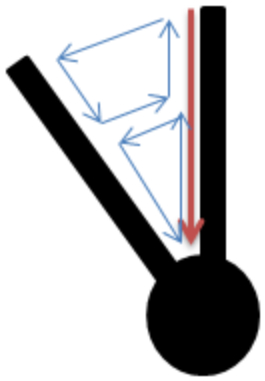

Figure 12. Convection occurring from radial forces.

Chapter 3. Methodology

This section discusses details of the experimental methods and the design of the testing apparatus, calculations, and design of the magnetic arrays and turbines. The *Overview of Experiments* provides a narrative to the experiments conducted. The section *Modeling and Verification of Magnet Performance* and *Design of Turbines and Performance Evaluation under Pigging Constraints* details the testing of the Halbach array and turbines. The *Overall Energy Balance of EM-Pig in Operation* section provides a conceptual framework for how the EM-pig will operate in the field.

Overview of Experiments

This section provides an overview of the experiments conducted and the methods used to analyze the data. The flow chart in Figure 13 shows the basic structure of the experimental plan. The rest of the section refers to this flow diagram. The sections *Magnet Testing*, *Turbine Testing*, and *Coupled Testing* provide the narrative for the corresponding sections in Figure 13.

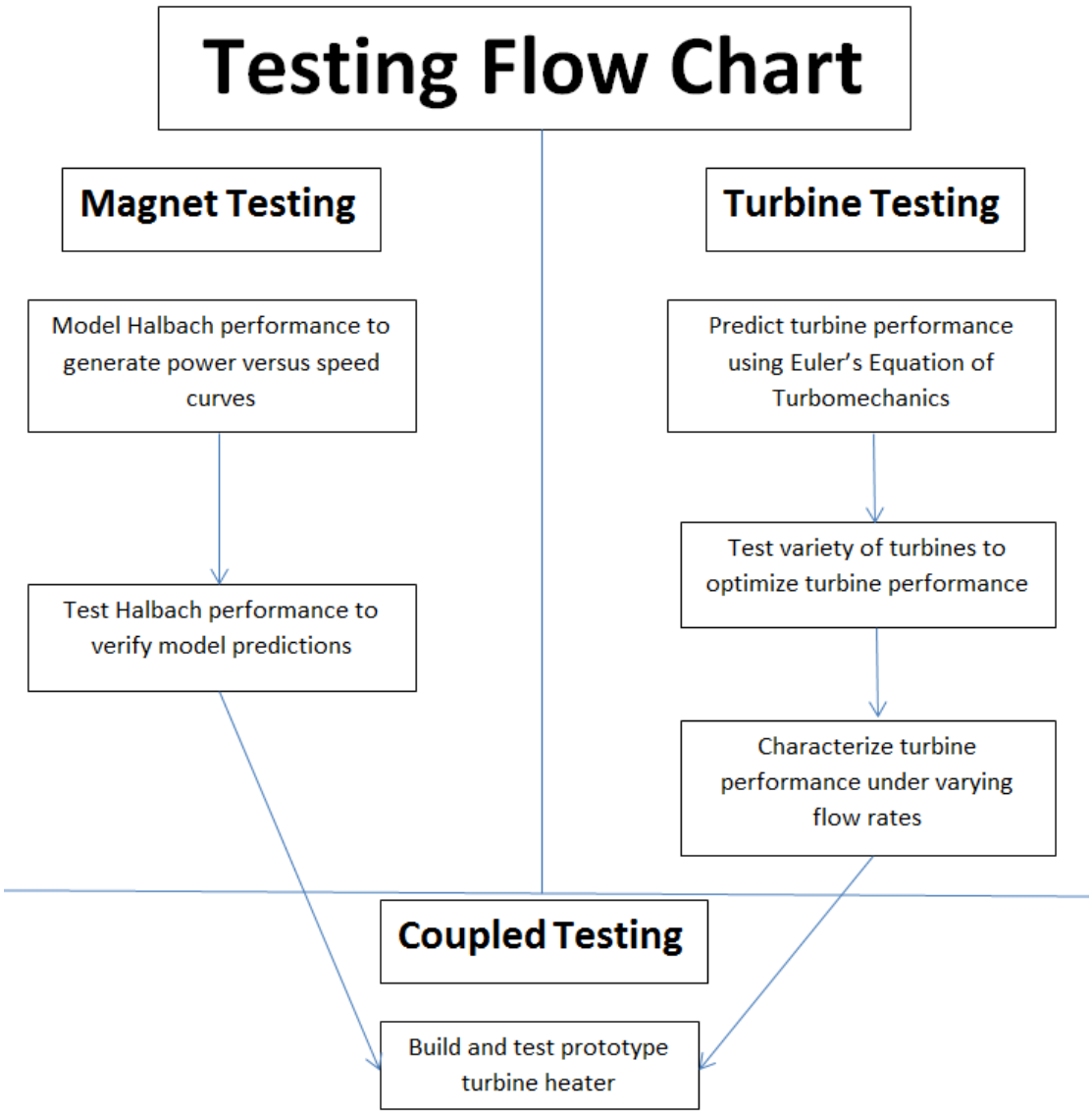

Figure 13. Testing Methodology Flow Chart.

Magnet Testing

The aim of the magnetic testing is two-fold. First is to understand the Halbach performance so a Halbach array with similar performance to the turbines could be built. Second, this Halbach array needed to be built and tested against the model.

Halbach Modeling

Computational modeling of the Halbach array is a fast and inexpensive way to chart the magnetic array performance. The aim was not just to understand the performance but was to

use this understanding to develop an array that could be powered by the turbines in the lab set up. The results of the modeling could provide a direction for the sizing and design for the Halbach array to be used later.

Halbach Physical Testing

While modeling can chart performance quickly and efficiently, lab testing was still necessary to corroborate the results. The real test data on the specific Halbach array performance allowed for confident matching to the turbines. The Halbach array testing produced a performance curve similar to Figure 14.

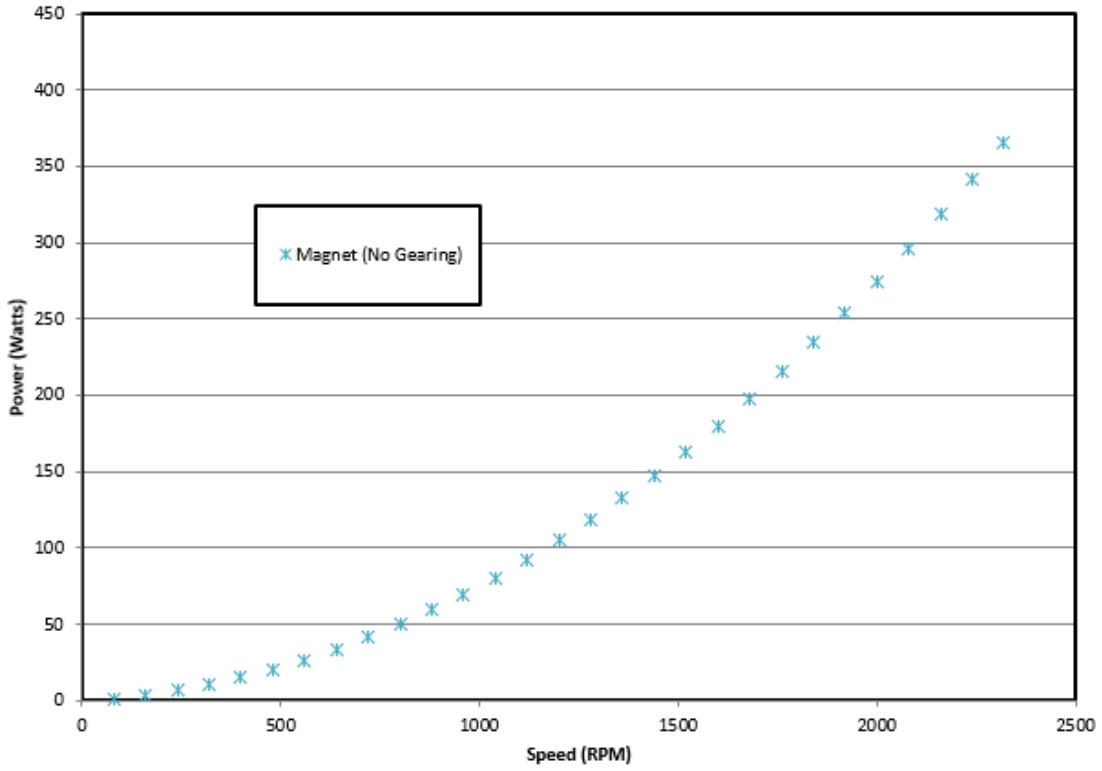

Figure 14. Halbach Performance Curve.

Turbine Testing

Unlike the magnetic testing with the Halbach array, the design of the turbines used had not been established, so extra steps were taken for the design. The aim of the turbine design and testing is to:

- Build a relatively efficient turbine.

    - Build one that is compatible with the Halbach array performance.
- Develop a methodology to design turbines based on desired performance.
    - Helps in scale up as this allows the user to design a turbine based on performance for a given flow rate, power, and using different working fluids.

Performance Driven Design

One of the aims of the turbine testing was to develop a methodology to design turbines based on the performance desired by the user. This was accomplished using an analytical method. A finite element model (FEM) was not used as numeric methods are well suited to determine the performance of a particular turbine, but not for design based on the desired performance. Furthermore, a FEM approach would require a moving mesh model which was beyond the scope of this study.

Optimizing Design Using Testing

The analytical method was able to provide many designs for a turbine with a particular performance. Because of the underlying assumptions and the limitations of the analytical approach, not all of the designs would provide the expected performance. Physical testing allowed for fine tuning of design parameters to achieve adequate and predictable performance. At the end of optimization testing, one turbine was selected to move on for further testing.

Variable Flow Rate Testing

The best performing turbine was run at varying flow rates. These tests provide a comprehensive performance map which simulates realistic pipeline conditions where flow rate will be changing. The variable flow rate testing produced a performance curve similar to the one seen in Figure 15. The red, green, and purple curves are the low, mid, and high flow rate tests, respectively.

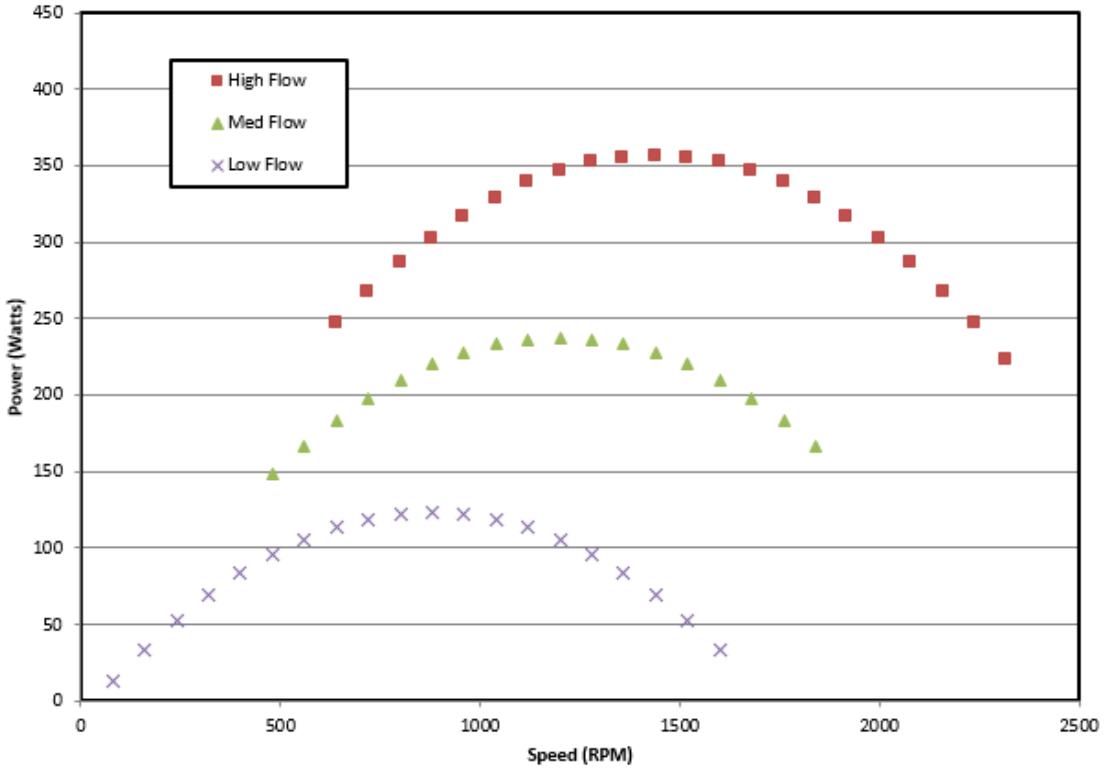

Figure 15. Variable Flow Rate Performance Curves.

Coupled Testing

The objective of the coupled testing was to produce a functional EM heater; this required matching the performance of the turbine and the Halbach array. Overlapping the two performance curves in Figure 14 and Figure 15 displays a situation similar to Figure 16. The coupled turbine and heater should produce power at the intersection of the Halbach and turbine curves. In Figure 16, the intersection of the curves is not close to the maximum power outputs for the turbine, especially at the mid and high flow rate tests.

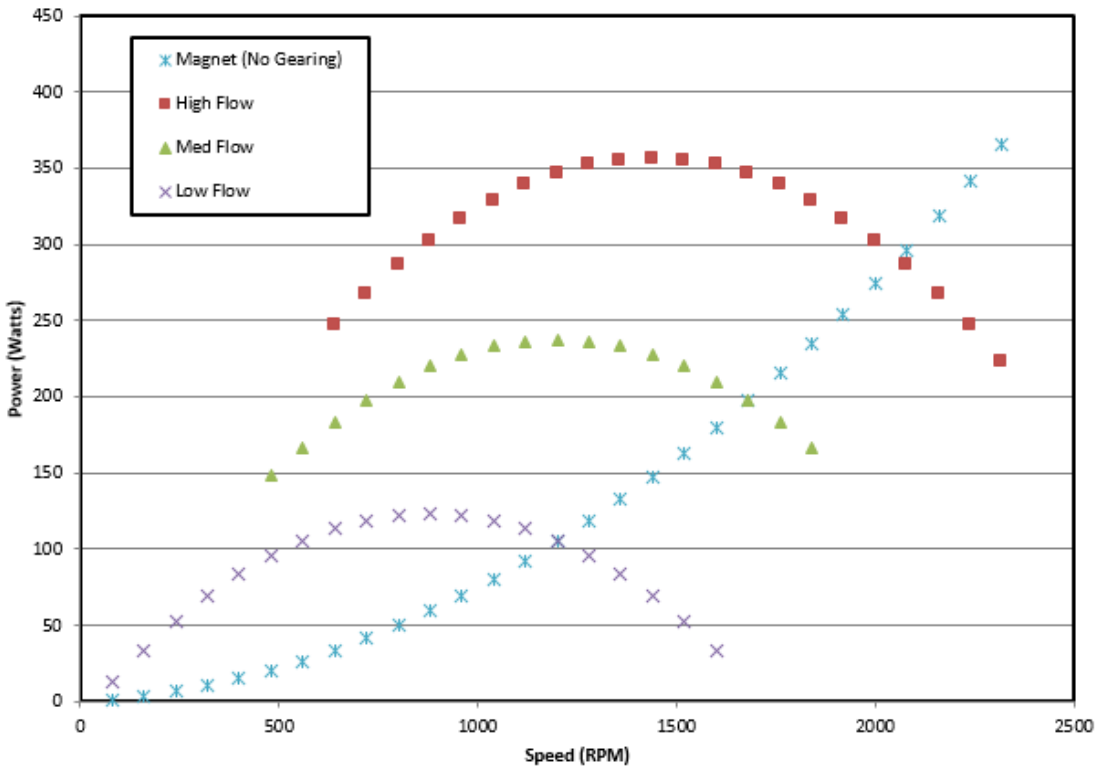

Figure 16. Overlaid Halbach/turbine performance.

This poor overlap between magnet and turbine perfomances indicates that the turbine and Halbach array need a gear ratio to match them. The effect of the gear ratio is to stretch or narrow the Halbach curve. A properly geared system looks like Figure 17.

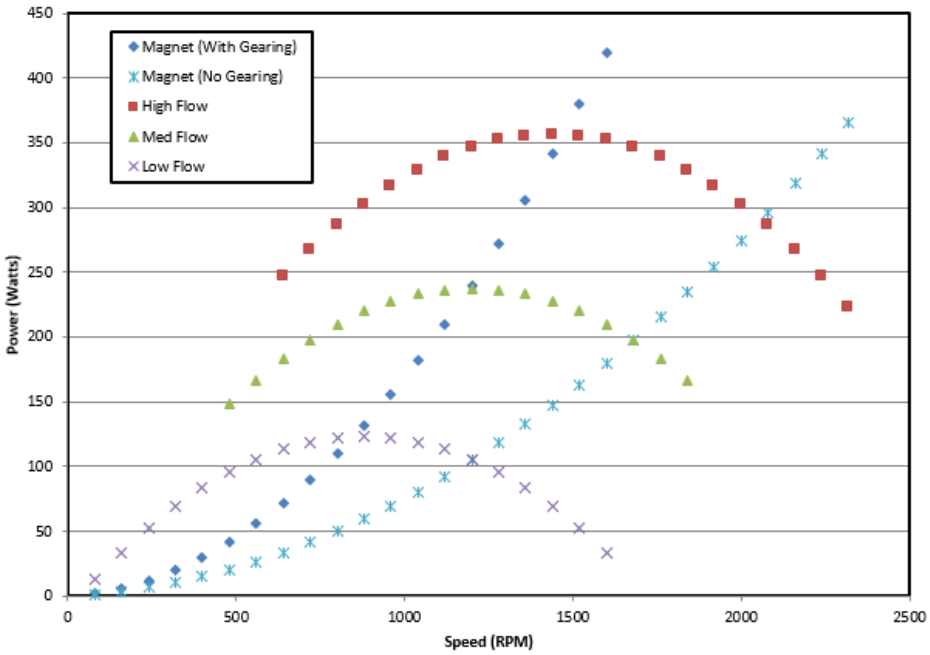

Figure 17. Overlay with gear ratio.

In a properly geared system, the two curves should intersect near the peak power of the turbines, see Figure 18.

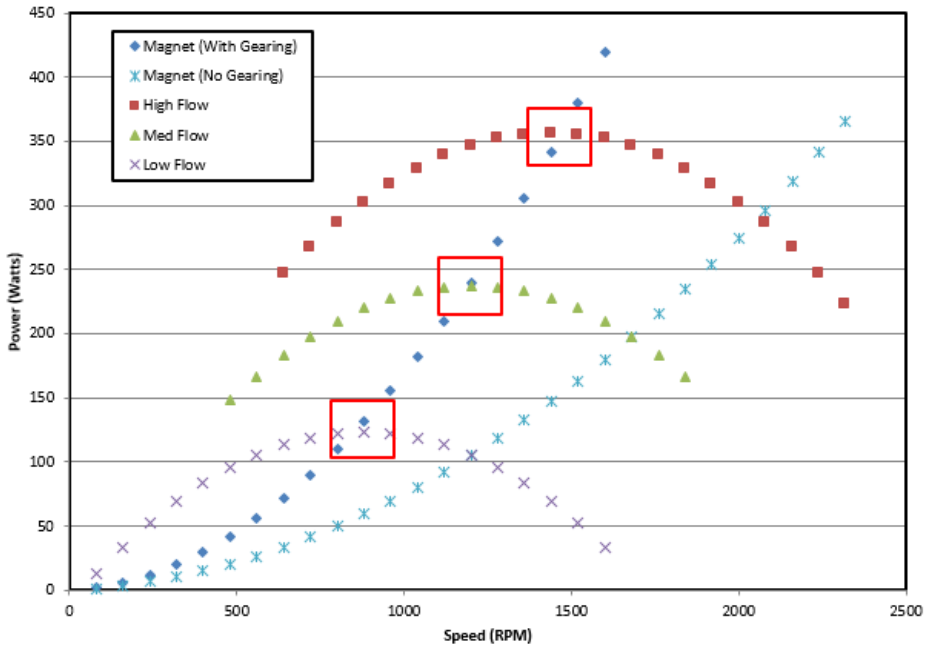

Figure 18. Overlay with highlighted intersections.

This prediction of the system performance seen in Figure 18 was then tested in a coupled test where the turbines and Halbach array were geared together.

Modeling and Verification of Magnet Performance

The goals of the magnet testing, covered in *Overview of Experiments*, are to characterize the Halbach performance with varying magnet array and pipe properties, and to build and characterize the performance of a Halbach array for use in a prototype heater. The section describes the procedure in the numeric modeling of the Halbach array to map the performance curves under varying parameters in *Modeling using Ansys*. The section *Experimental Verification* covers the experimental procedure to verify the work done in the models and characterize the performance of the Halbach array which would be used for the coupled test.

Modeling using Ansys

Modeling allows for fast and efficient testing on the Halbach performance. This ability to run many tests quickly allowed studies of multiple parameters to be run. This section covers the inputs for the model simulation along with the test matrix.

Procedure

The Halbach array was drawn into Ansys, and the heat dissipation could be modeled by calculating the magnetic flux change through the aluminum pipe. Figure 19 shows the model used in the Ansys simulation. The magnetic lobes can be seen. These nodes vary the magnetic field strength within the pipe wall which is responsible for the inductive heating. These models were run by Clay Hearn of the University of Texas's Center of Electromechanics.

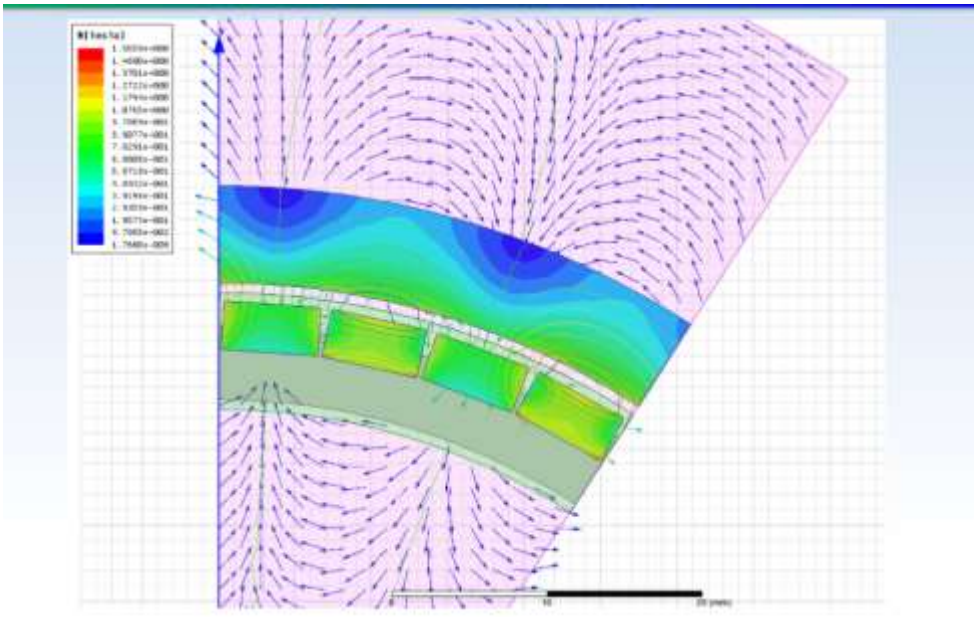

Figure 19. Halbach Ansys Model.

Test Matrix

The tests were a run on a base using the parameters shown in Table 3:

Table 3. Halbach Ansys test matrix with base values bolded.

Test Parameter	Value
Pipe ID	3in,**4 in**, and 6in
Pipe Wall Thickness	0.125in, **0.25in**, and 0.375in
Pipe Material	**Steel** and Aluminum
Air Gap	0.025in, **0.05in**, and 0.1in
Magnet Speed	100RPM, **200RPM**, 400RPM, 800RPM, and 1600RPM

In each of the sensitivity tests, one of the above parameters was changed to see the effect that the modified parameter had on the heat generated.

Experimental Verification

The experimental verification step required building a Halbach array and housing it inside an aluminum pipe, similar to the model simulated in Ansys. A basic design for the experimental test bed was to place the array and pipe inside a calorimeter to measure the heat produced over a period of time. The design and procedure of this trial can be found in the sections *Materials/Setup* and *Procedure*.

Materials/Setup

The experimental setup needed to meet certain design criteria are:

- House the magnet array and pipe
    - Up to 1500 RPM
- Small heat loss
    - Small heatlosses reduce error in calulations and makes the measurements more repeatable
- Accurately measure shaft speed

Based on these standards, the design of the testbed was built of two concentric pipes, the inner pipe being the aluminum pipe and the outer pipe was acrylic. The annulus between these two pipes was filled with water which would conduct heat away from the aluminum pipe. Fiberglass insulation was wrapped around outside of the acrylic pipe reducing heat loss to the environment. A cap was installed to sit on the surface of the water for heat loss reasons, as well. Warm water will lose heat from evaporative cooling. Introducing a cap, seen as blue in Figure 20, limits how much cooling can occur during the test. A picture of the experimental setup can be seen in Figure 20.

Figure 20. Halbach Heating Test Set-Up.

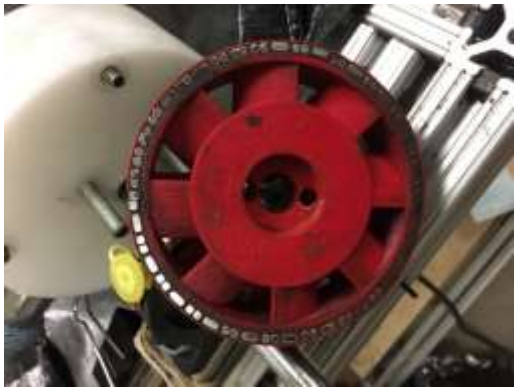

Figure 21. Halbach array used in Halbach and coupled testing.

A thermocouple was inserted into the water to measure the temperature during the test, and an optical tachometer measured shaft speed. The shaft was driven by a drill press and was held in place on the bottom by a bushing.

Fiberglass has a thermal conductivity of $0.04\frac{W}{m*K}$, so a half inch section of insulation would have an average heat loss can be estimated around 4 Watts (Smith et al., 1981). This was sufficiently low for so as not to interfere with the expected heat generation rates of 200-400 Watts.

Power Calculations

The temperature rise in the water was used to calculate the power using the heat capacity of water.

$$q = m * C_p * \Delta T$$

[10]

$$P = \frac{q}{t} = \frac{m * C_p * \Delta T}{t}$$

[11]

Where:

q is heat demand (Joules)

m is mass (kg)

C_p is heat capacity ($\frac{J}{kg*T}$)

ΔT is change in temperature (K)

P is power requirement (Watts)

t is time (s)

Procedure

The procedure for this experiment was as follows:

1. Wear safety glasses.
2. Verify that the base of the calorimeter is secured to the drill press.
3. Select drill press shaft speed by changing pulley arrangement.
4. Read water temperature on thermocouple read-out. Record temperature.
5. Turn on the drill press and start the clock.
6. Measure shaft speed using an optical tachometer. Record.
7. Wait until the test has run for 10 minutes. Shut off drill press.
8. Wait for temperature in a water bath to equilibrate. Record final temperature.
9. Remove calorimeter and pour water into graduated cylinder. Record volume.
10. Fill calorimeter back up with water.

11. Reinstall onto drill press.
12. Repeat steps 2-11 for all shaft speeds possible on the drill press.

Design of Turbines and Performance Evaluation under Pigging Constraints

When designing a turbine for a particular pipeline with a known flow rate, it is valuable to have a methodology that can predictably produce a turbine to achieve a given power. This section covers the process used to determine the turbine geometry, how to accurately produce that turbine geometry, and designing the test set up to evaluate the turbine performance.

Performance Driven Turbine Design

Performance driven turbine design is the process of using performance inputs such as target power output, pipeline flow rates, pigging speed, and paraffin deposition to produce a turbine geometry. Once this turbine geometry is calculated, the turbine can be drawn into an AutoCAD software before being constructed using 3D printing processes.

Using Euler's Equations to Develop Blade Geometry

Euler's equation and radial equilibrium theory are the two fundamental equations dictating turbine geometry. This section covers the methodology of how turbine geometry was calculated based on target power output, pipeline flow rates, pigging speed and paraffin deposition.

Determination of Torque and Speed Requirements

The torque that the turbine will operate at can be found if the power and operating speed are known.

$$P = \tau * \omega \quad , \ \tau = P/\omega$$

[12]

Where

P is power (Watts)

τ is torque (N*m)

ω angular speed (rad/s)

Power is known as it is an user input, which can be determined using the heating needed to solubilize the paraffin for the particular pipeline. The angular velocity is also selected as a user-defined input. However, a few considerations should be taken into account when choosing the turbine operating speed; namely specific speed and reasonable gearing ratio.

The specific speed of a turbine is defined as:

$$n_s = \frac{n*\sqrt{P}}{H^{\frac{5}{4}}}$$

[13]

Where:

n angular speed (RPM)

P is power (kW)

H is pressure drop or head (meters)

The consensus is that propeller type axial turbines perform best at specific speeds between 100 and 200 (White, 2011) (Turton, 1995). When determining operating speed of the turbine, select a speed that puts the specific speed of the turbine within the 100-200 window. If the speed is unreasonably high, consider breaking the turbine into multiple stages as this decreases the head drop over the stage and increases the specific speed.

If the turbine speed is too high, it could make gearing the turbine to the Halbach array complicated. The rate at which the magnet array spins at is determined by the heat rate and the power-speed relationship for the particular Halbach array. If the turbine has a much higher angular velocity than the magnet array, large gears ratios are needed to gear down the speed. This may not be feasible in with the space constraints in the pig.

Blade Angle Design

Once the torque, angular speed, flow rate, and oil density are known the blade angles can be determined from radial equilibrium theory.

Radial equilibrium states that:

$$V_{\mu\ inlet} * r^n = c$$

[14]

"c" is not defined, though it can determined through calculation. Since V_μ on the outlet of the rotor is 0, $\Delta V_\mu = V_{\mu\ inlet}$ or $\Delta V_\mu = \frac{c}{r^n}$

The torque acting on a dr thick section of blade distance r from the axis of rotation can then be expressed as:

$$d\tau = c * V_a * 2\pi * \rho * r^{2-n} dr$$

[15]

Integration of the equation above from the hub radius to the outer radius, which are both user inputs:

$$\tau = c * V_a * 2\pi * \frac{\rho}{2-n} * [{r_{outer}}^{3-n} - {r_{hub}}^{3-n}]$$

[16]

The expression can be rearranged as:

$$c = \tau * \frac{2-n}{[V_a \pi \rho ({r_{outer}}^{3-n} - {r_{hub}}^{3-n})]}$$

[17]

Where:

c is the blade twist constant

τ is torque (N*m)

n is degree of free vortex where n=1 is free vortex

V_a is velocity in the axial direction or velocity fluid is traveling down the pipe (m/s)

ρ is the density of the working fluid (kg/m^3)

r_{outer} is the radius of the blade tip (m)

r_{hub} is the hub radius (m)

Now using equation [17], the inlet and outlet blade angles for both the stator and rotor can be solved, where α_2 and α_1 are the inlet and outlet blade angles for the stator, respectively and β_1 and β_2 are the rotor inlet and outlet blade angles, respectively. Refer to Figure 22 for the blade angles.

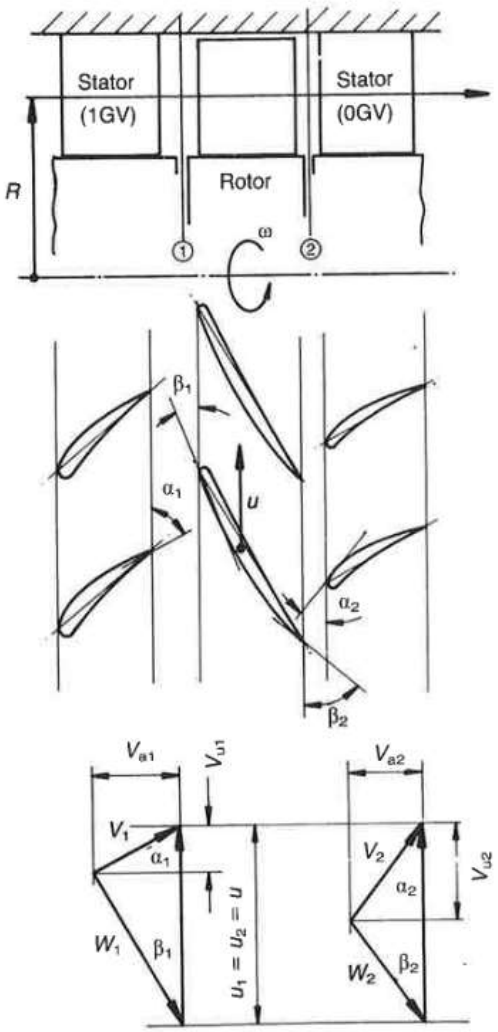

Figure 22. Stator/Rotor Diagram with Blade Angles (Turton, 1995).

Outlet Velocity Triangle:

Since the flow is leaving without swirl, the outlet flow is normal to the rotation of the turbine and $\alpha_2$is 90 degrees, as seen in Figure 23.

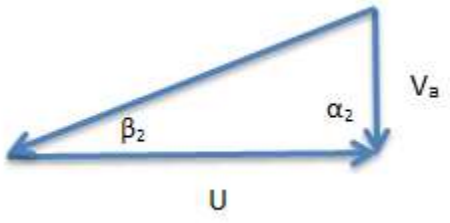

Figure 23. Outlet velocity triangle.

$\beta_2$can be expressed as $\tan^{-1}\left(\frac{V_a}{U}\right)$. Since U is the tangential velocity of the rotor at distance "r", the expression can be replaced with β_2 =$\tan^{-1}\left(\frac{V_a}{\omega r}\right)$.

Inlet Velocity Triangle

In the inlet velocity triangle, the flow has a velocity component in the same direction as the movement of the rotor (ΔV_μ). The inlet velocity diagram looks as follows:

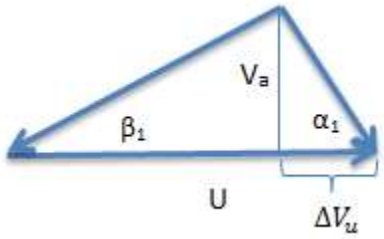

Figure 24. Inlet velocity triangle.

α_1 can be solved as $\tan^{-1}\left(\frac{V_a}{\Delta V_\mu}\right)$ and replacing V_u with $\frac{c}{r^n}$ the expression can be shown as:

$$\alpha_1 = \tan^{-1}\left(V_a \frac{r^n}{c}\right)$$

[18]

β_1 can be solved as $\tan^{-1}\left(\frac{V_a}{U-\Delta V_\mu}\right)$. After replacing U and (ΔV_μ), the expression becomes:

$$\beta_1 = \tan^{-1}\left(\frac{V_a}{\omega r - \frac{c}{r^n}}\right)$$

[19]

This process using equations [19], [17], [14], and [13] has been written into an excel program which can take a variety of user inputs to determine the blade angles at varying blade radii. A screenshot of the spreadsheet can be seen in *A- Methodology* (Figure 51).

Implementation of Design through SolidWorks

The blade angles of the rotor and stator calculated in the previous section need to be drawn into a 3D model so it can be constructed using 3D printing. This section outlines the methodology used to render the turbine rotor and stator in SolidWorks.

Rendering Blade Geometry

The blade geometry is important to the overall design of the turbine as it is the component that works to drive the rotor/stator pair. The turbine blades were drawn one of two ways depending on the relative length of the blade. Blades that were less than 30% of the radius length have a static cross-section. Blades with longer profiles were drawn with changing cross-sections. The processes for drawing the geometries are described in this section.

Short Blade Process

As described in *Blade Angle Design*, a blade in radial equilibrium has blade angles which vary with the blade length. However, the process, which is outlined in *Long Blade Process*, to draw a number of blade profiles on several planes can be time intensive. With turbines that have short blades, especially if they are far from the axis of rotation, the blade angles do not vary much.

Blade Profile									
r/R	ΔVu	Vu_in	Vu_out	U	α1	α2	β1	β2	Degree of Reaction
0.1	4.00	4.00421	0.00	1.13	33.67	#DIV/0!	-42.87	67.03	-5.285
0.15	4.00	4.00421	0.00	1.70	33.67	#DIV/0!	-49.13	57.56	1.687
0.2	4.00	4.00421	0.00	2.26	33.67	#DIV/0!	-56.83	49.72	0.897
0.25	4.00	4.00421	0.00	2.83	33.67	#DIV/0!	-66.17	43.55	0.676
0.3	4.00	4.00421	0.00	3.39	33.67	#DIV/0!	-77.06	38.19	0.579
0.35	4.00	4.00421	0.00	3.96	33.67	#DIV/0!	-88.98	33.99	0.529
0.4	4.00	4.00421	0.00	4.52	33.67	#DIV/0!	79.02	30.54	0.501
0.45	4.00	4.00421	0.00	5.09	33.67	#DIV/0!	67.91	27.67	0.483
0.5	4.00	4.00421	0.00	5.65	33.67	#DIV/0!	58.29	25.26	0.473
0.55	4.00	4.00421	0.00	6.22	33.67	#DIV/0!	50.32	23.22	0.466
0.6	4.00	4.00421	0.00	6.78	33.67	#DIV/0!	43.83	21.47	0.461
0.65	4.00	4.00421	0.00	7.35	33.67	#DIV/0!	38.58	19.95	0.459
0.7	4.00	4.00421	0.00	7.91	33.67	#DIV/0!	34.31	18.63	0.457
0.75	4.00	4.00421	0.00	8.48	33.67	#DIV/0!	30.80	17.46	0.456
0.8	4.00	4.00421	0.00	9.04	33.67	#DIV/0!	27.89	16.43	0.456
0.85	4.00	4.00421	0.00	9.61	33.67	#DIV/0!	25.45	15.51	0.456
0.9	4.00	4.00421	0.00	10.17	33.67	#DIV/0!	23.38	14.69	0.456
0.95	4.00	4.00421	0.00	10.74	33.67	#DIV/0!	21.61	13.95	0.456
1	4.00	4.00421	0.00	11.30	33.67	#DIV/0!	20.07	13.28	0.457

Figure 25. Example Calculation of Short Blade Turbine.

In Figure 25, the blade angles used are from $(\frac{r}{R} = 0.75 \ \ to \ 0.9)$ as seen by the shading on column 1. α_1 and α_2 do not vary at all. β_1 varies from 30.80º to 23.38º. β_2 varies from 17.46º

to 14.69º. The small variation in blade angle allows for a median value to be used for the entire blade length. Once the blade angles are averaged, they are drawn into a shape on SolidWorks and the shape is extruded from that cross section, see Figure 26.

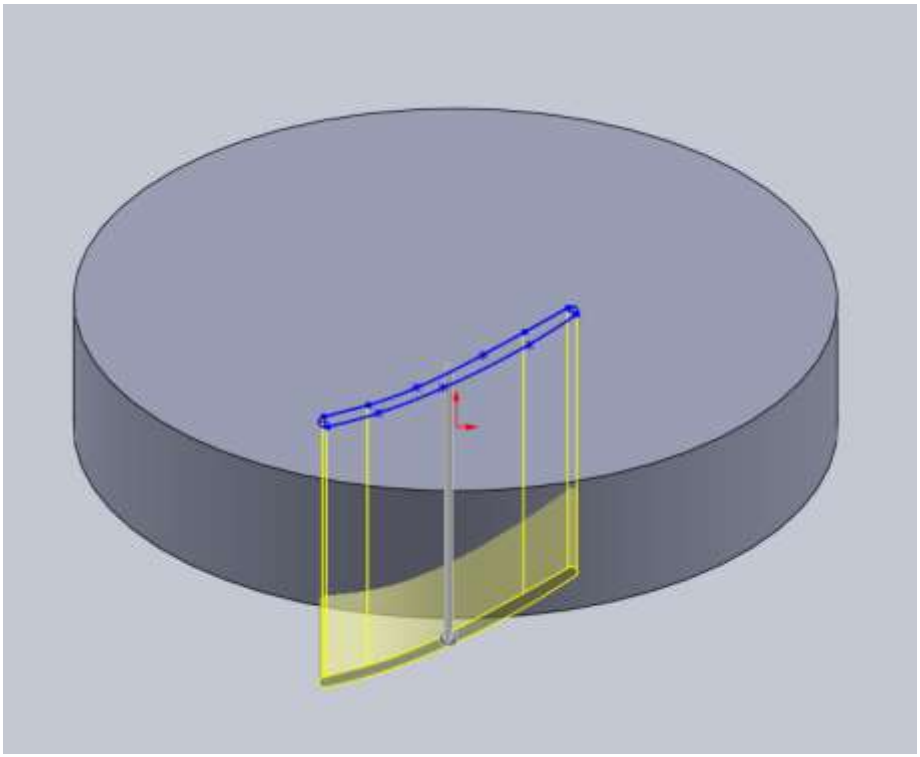

Figure 26. Blade Being Extruded From Single Shape.

Long Blade Process

In turbine blades that are long (greater than 30% of the total blade radius), the long blade process was used to render the blade shape. Rather than using one cross-section to extrude the entire blade, the long blade process would draw several cross-sections on parallel planes. Each cross-section would be drawn with blade angles correlating to the radius that the plane corresponded with. Once the correct blade shapes were drawn, they would be rendered into a 3D shape using the "Loft" function in SolidWorks. The Loft function creates an object between two shapes by transitioning the cross-sections between the two reference shapes. The result can be seen in Figure 27.

This process produces a blade geometry much closer to the profile called for in *Blade Angle Design*. However, this process could take several hours as each profile needs to be similar enough to each other so that the lofting process creates a seamless blade shape.

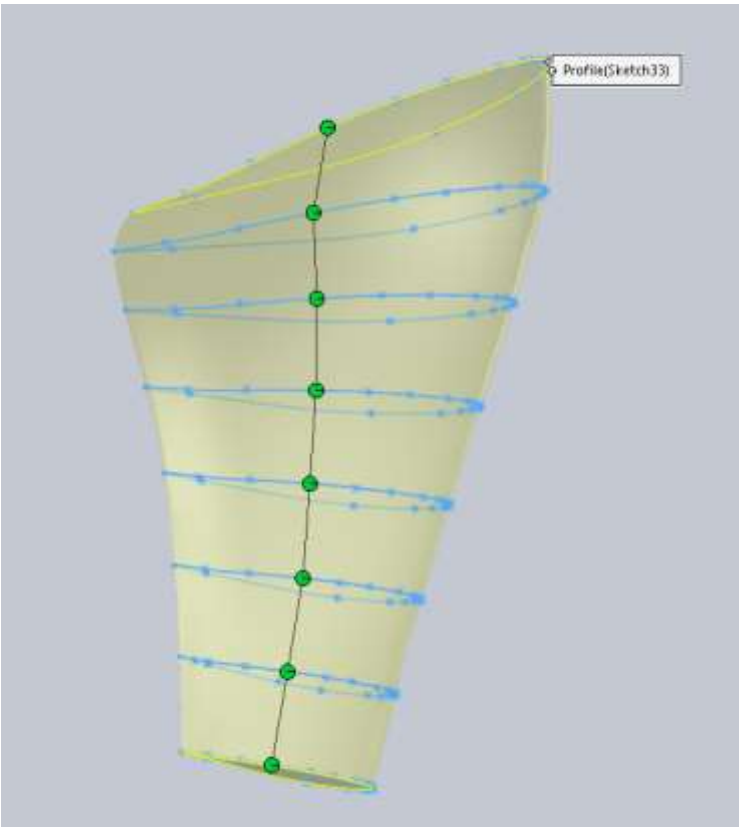

Figure 27. Long Blade being Lofted.

Building Turbine Shape from Single Blade

The process of taking a single blade and building the entire turbine is relatively straight forward:

1. The blade was copied in a circular pattern around the axis of rotation.
2. The excess blade is trimmed to the final diameter of the turbine.
3. The hub of the turbine is extruded from a circle.
4. Features are removed from the center to allow for the turbine to mate to the drive shaft.
5. Features, like a nose cone, are added to make the shape more hydrodynamic

Examples of the final result are shown in Figure 29 or **..**

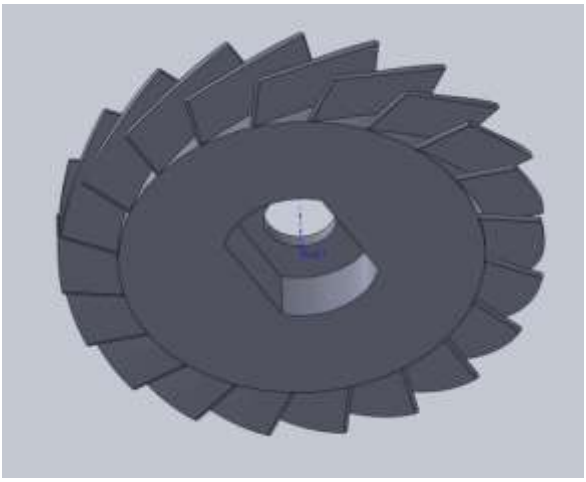

Figure 28. Lofted Long Blade Turbine (Right).

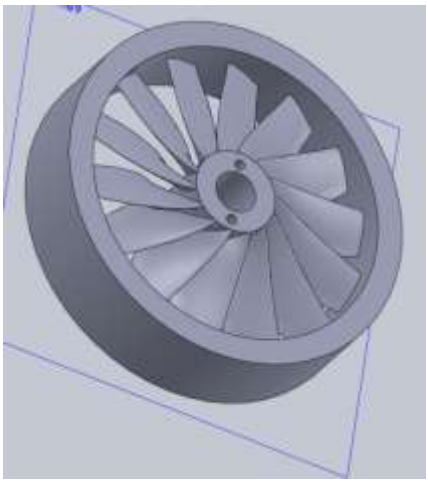

Figure 29. Extruded Short Blade Turbine.

3D Printing Prototypes

The 3D printer, MakerBot, uses the STL file to render the shape on the MakerBot program (see Figure 30). The data can then be exported to the printer and printed in a matter of minutes to hours, depending on object size and complexity.

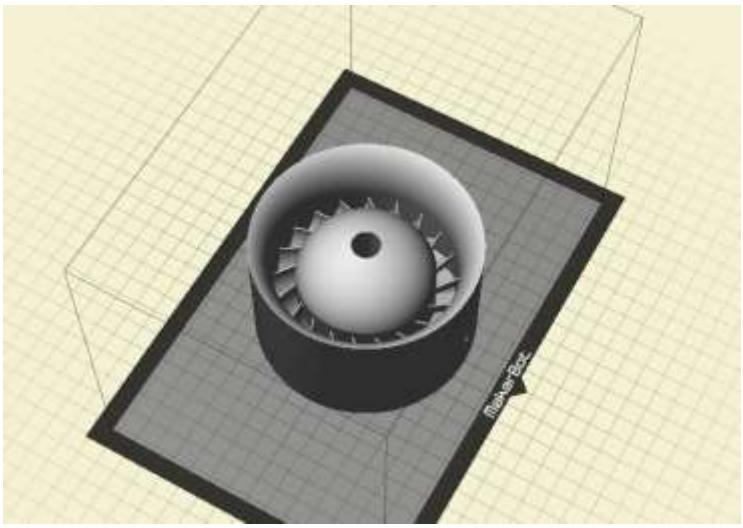

Figure 30. 3D Rendering of turbine stator on 3D printing program.

Performance Evaluation Under Pigging Conditions

Fabricating the turbines is only the first step. Once built the turbines needed a test bed to evaluate their performance. This section details the test bed design and the test matrix for the turbines performance evaluation.

Test Set Up

The test bed for the turbine performance must meet certain design criteria:

1. Provide adequate flow for turbines
    - The specific speed calculations were used to determine that a 100 Watt propeller turbine needs a flow rate of at least 60GPM
    - Flow distribution at inlet of turbine should be uniform
2. Ability to switch out turbines frequently
    - Since many turbines were tested, the test bed should be built to accommodate multiple installations.
3. Small shaft friction
    - The propeller type turbines operate at high speeds and low torque. The maximum torque produced is about 1 N*m. The friction in the system should be small relative to the torque produced (<0.25N*m)
4. Accurately measure shaft power and speed

- Since the power performance curves were the metric which the turbine performance was evaluated, the test bed needed to measure the shaft power delivered by the turbine accurately.

5. Must be able to vary flow rate through turbine
    - Since the flow rate through the pig will change with the flow rate through the pipeline and the pig velocity, a test bed to simulate infield flow conditions needed to have the ability to alter the flow rate through the turbine

The general schematic of the test bed can be seen in Figure 31.

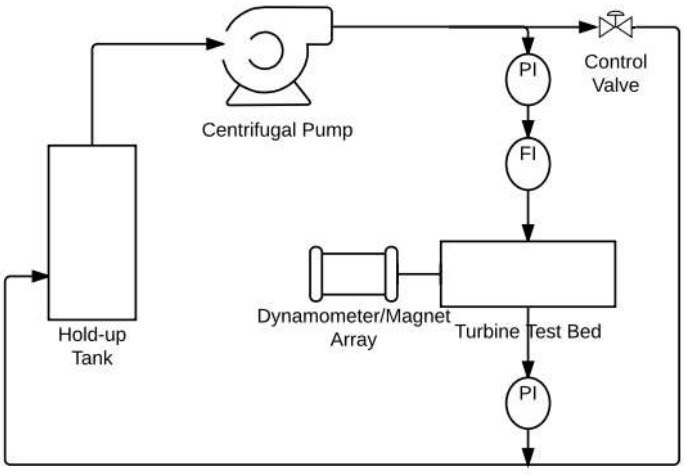

Figure 31. Test Bed Schematic.

The design solution for Criterion 5 can be seen in Figure 31. Flow can be throttled by controlling the flow rate through the pump, or by controlling a bypass to divert a portion of the flow rate from the test bed. The pump speed on an AC electric pump can be throttled with a Variable Frequency Drive or VFD. These have an associated cost and require tuning for a particular pump. For these reasons, the by-pass option was chosen. The drawback of this option is that the flow rate through the turbine cannot be throttled to zero, or near zero, flow rates. This drawback was deemed manageable as the dynamometer may not be able to measure the power at these flow rates accurately.

The solutions for other design criteria are covered in the following sections; *Flow Loop Design*, *Turbine Housing Design*, *Dynamometer Design*, and *EM Heater Design*.

Flow Loop Design

The flow loop design will encompass all components in Figure 31 that are not the turbine test bed and the Dynamometer/Magnet Array. These components are the centrifugal pump, pressure indicators, flow indicators, hold-up tank, control valve, and flow lines.

Centrifugal Pump

A centrifugal pump was the chosen pump type as they are relatively inexpensive for their performance and are a readily available pump type. They do have a few design drawbacks that were addressed in the inlet design. First, they are not self-priming which requires the pump to be lower than the water level in the holding tank, so the inlet line remains primed with water during startup. Second is the tendency for this pump type to cavitate. The pump manufacturers provide a maximum inlet pipe length to maintain sufficient net positive suction head, $NSPH_R$. Keeping the suction line short enough and installing the pump lower than the water level were the two considerations when installing the centrifugal pump.

With these considerations in mind, the Red Lion RSLP-200 centrifugal pump was chosen. This model's pump curves showed the Red Lion RSLP-200 would be able to provide 75-80GPM flow rates at the expected pressure drops. This is more than the 60GPM criterion for the flow rate.

Pressure Indicators

The pressure indicator needed to measure the pressure drop across the turbine for efficiency calculations. A Dwyer DPGA-06 pressure indicator was used, as it had 1% accuracy and would be able to measure the 0-25 psi pressures in the flow loop; see Figure 32.

Figure 32. Dwyer Pressure Gauge. **(Dwyer Instruments, 2017.)**

Flow Indicator

The flow indicator was used in the experiments to calculate efficiency, and benchmark performance between turbines in the variable flowrate tests. Commercial options for inline flow meters were costly, so a method to measure flow rate was devised. The flow through the turbine was diverted into a separate tank for a known period. A scale tarred to the empty tank weight would measure the change in mass of the tank. This change in weight was used to calculate the flow rate:

$$\dot{V} = \frac{m_2 - m_1}{\rho * t}$$

[20]

Where:

$\dot{V}$ is the volumetric flow rate (m^3/s)

m is the mass of the tank (kg)

ρ is the density of the fluid (kg/m^3)

t is time (s)

Hold-Up Tank

The holdup tank is required in a pump flow loop. A 25-gallon barrel was used for the flow loop. The 25-gallon volume was large enough for a 10-second flow rate test, so the tank passed all criteria.

Control Valve

A 1.5in linear gate valve was used for the control valve. Linear globe valves provide linear flow resistance on the openness of the valve. This allows for proper control of the by-pass flow rate.

Flow Lines

The flow line size in the test bed was based on the Darcy-Weisbach equation:

$$\frac{\Delta p}{L} = f_D * \frac{\rho}{2} * \frac{\bar{v}^2}{D}$$

[21]

Where:

$\frac{\Delta p}{L}$ is the frictional pressure gradient (Pa/m)

f_D is the Darcy friction factor

ρ is the density of the fluid (kg/m^3)

$\bar{v}$ mean velocity of the pipe flow (m/s)

D the hydraulic diameter of the pipe (m)

Based on the expected flow rates, a 1.5in line would keep the total pressure drop through the system under 3psi, which is small enough not to impact the pump flow rate significantly.

Turbine Housing Design

The turbine housing is the piece of test equipment that contains the turbine. The design criteria dictate that the turbine housing needs to provide uniform flow to the turbine (criterion 1), allow for installation of several turbines (criterion 2), and have small shaft friction (criterion 3).

The basic design of the turbine housing was an 18 in long 4.25in polycarbonate pipe with two end caps with flow ports and a center hole for the drive shaft to pass through, see Figure 33.

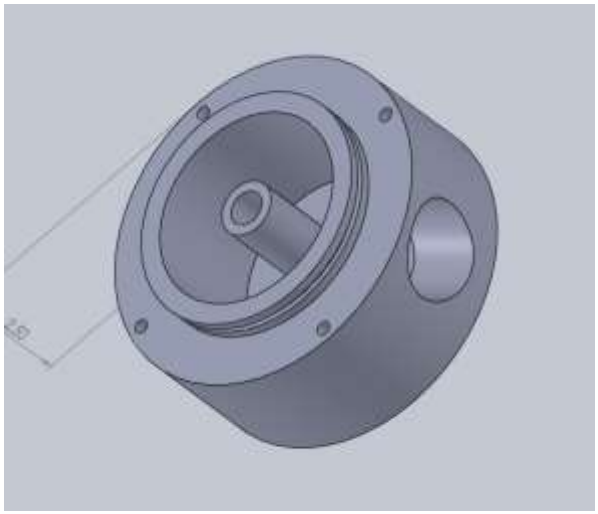

Figure 33. Turbine Housing Endcaps.

The details of how the turbine housing met design criteria 1,2, and 3 are found in the following sections.

Ensuring Uniform Flow Distribution

Turbine performance is dependent on the velocity flowing through the blades. If the flow distribution is not uniform throughout the turbine, the turbine will not perform as predicted and may decrease overall performance. When flow enters a different diameter pipe, the flow distribution is not uniform, and a particular entrance length is required to allow for the flow to fully develop. In turbulent flow, this could be from 20 to 100 pipe diameters or 6 feet to 30 feet. This pipe length is too long for the laboratory set up. To decrease the entrance length, diffuser plates can be installed to redistribute the flow.

A model of the diffuser plate flow housing was drawn in SolidWorks and imported into a CFD program. Simulations were run on the diffuser plate in the housing at 80GPM flow rates. The results can be seen below.

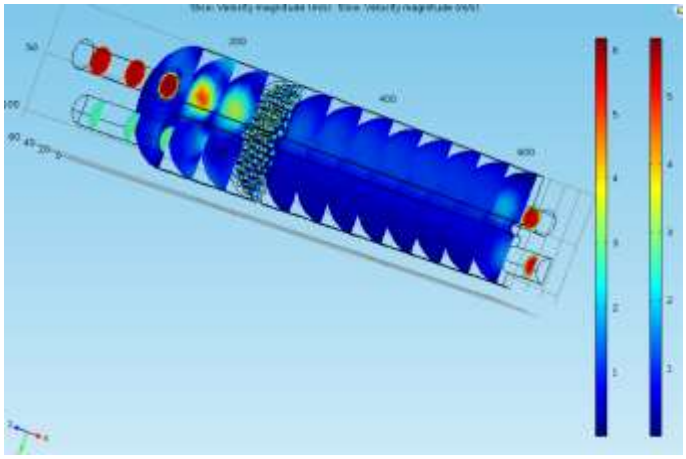

Figure 34. Flow Distribution with Diffuser Plate.

The CFD model shows uniform flow distribution with the diffuser plate. The tested diffuser plate model was then sent out to be laser cut out of $\frac{1}{4}$" acrylic sheet.

Low Shaft Friction

The expected torque produced by the turbines was expected to be around 1 N*m. If the shaft friction was too great, then this would limit the range of speeds the turbines could be tested. As a design criterion, we wanted to keep the friction in the housing to less than one-quarter of the maximum torque produced by the turbine (0.25 N*m). In each endcap low friction bushings were installed to keep the friction to a minimum.

After some trial and error, it was determined that the bushing alignment was critical to low shaft friction. In this two bearing system the friction of the bearings depends not just on the quality of the bearing, but the misalignment in the two bearings. Misalignment in the bearings impinges and flexes the shaft. The amount of deflection and the hardness of the shaft increase the normal force and thus friction inside of the bearings. Misalignment can occur in two modes, spatial misalignment, and angular misalignment. Spatial misalignment takes place when the bearings are misaligned in the x or y-direction. Angular misalignment happens when the bearings are not angled towards each other (See Figure 35). Several steps were taken to minimize the misalignment in the bearings.

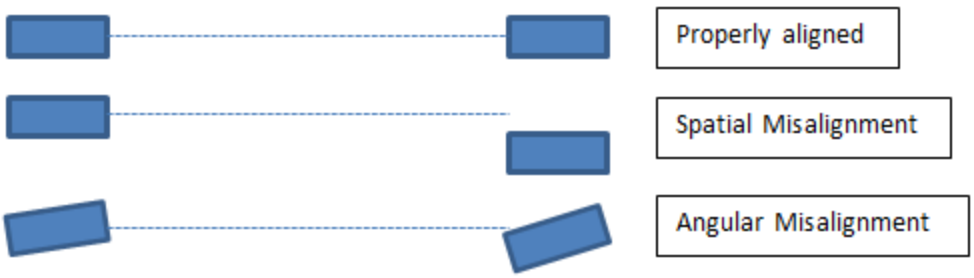

Figure 35. Types of Misalignment.

The angular misalignment of the bearings comes from the method in which the end caps are mounted about each other. Tightening the all-thread down made the ends of the pipe the two surfaces which the end caps were attached to. Unfortunately cutting the ends of the pipe so that they were both squares proved difficult to do on such a large pipe. So rather than trying to make the end of the pipe square, equal length pipes were placed over the all-thread rod. When the all-thread was tightened, the endcaps were pressed against the pipes rather than the un-square ends of the pipe (See Figure 36)

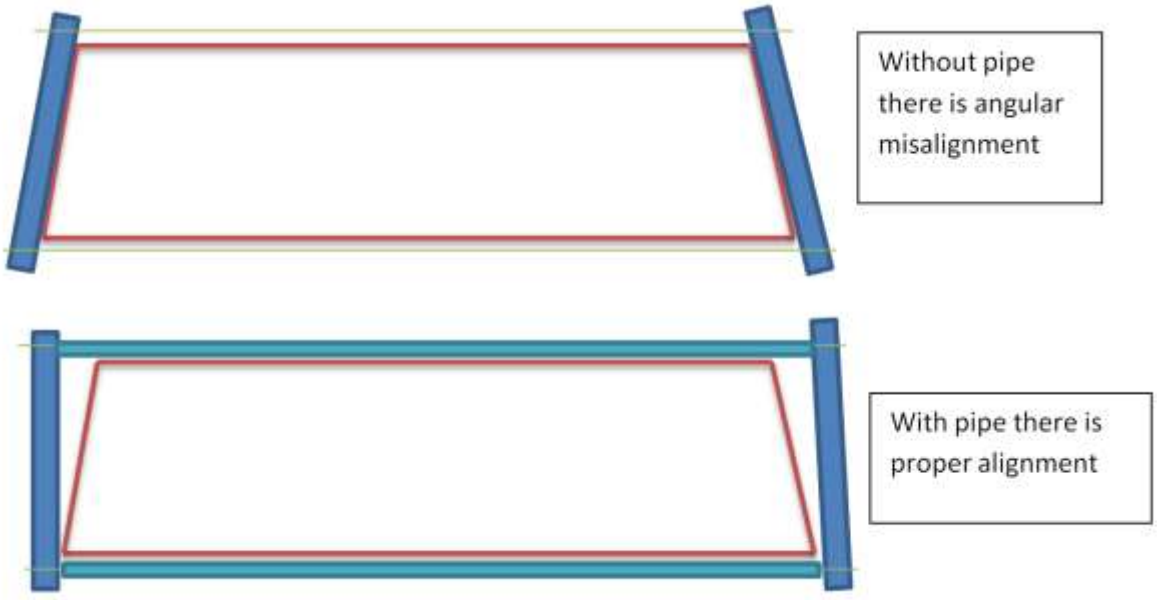

Figure 36. Diagram of misalignment from uneven ends.

Once these steps to control for misalignment were taken, the total shaft friction was measured at 0.1N*m which was well below the 0.25N*m benchmark.

Reinstalling Turbines

For many turbines to be installed in the test bed, the test bed design must allow for easy access to the turbine without attaching the turbine permanently.

The turbine is readily available as the whole assembly is held together by the all-thread rod. Accessing the turbine requires loosening the wing nuts and pulling off the endcaps. Attaching the turbines in a way that made them reusable utilized a method where the rotor would slide over a modified shaft collar, **.**. The shaft collar had two flat surfaces that would mate with the rotor and prevent rotation. The rotor would be held against the shaft collar by the water pressure. The rotor could easily be slid off the shaft to replace the rotor.

Dynamometer Design

The dynamometer measures the shaft power of the turbine. The dynamometer will need to measure a shaft power up to 300Watts at speeds up to 2500RPM. Commercially available dynamometers were prohibitively expensive, so a dynamometer was fabricated in-house. The dynamometer consisted of two parts, a braking wheel to apply a restraining torque and a tachometer to measure the speed at which the braking force was being overcome. The product of the torque applied and the speed is the measured shaft power.

The braking wheel consisted of a 6 inch wheel with a steel band to apply the braking force. The metal band was tensioned by a pair of calibrated spring scales, see Figure 37.

Figure 37. Braking wheel.

When the wheel spins, one of the springs increases in tension while the other decreases. The difference in the tensions is the frictional force on the wheel. The torque applied by the brake is found by using:

$$\tau_{applied} = \left|F_{spring1} - F_{spring2}\right| * r_{wheel}$$

[22]

Where:

$\tau_{applied}$ is the torque applied by the braking wheel (N*m)

F_{spring} is the tension in the spring scales (N)

r_{wheel} is the radius of the braking wheel (m)

The tachometer used was an optical tachometer with a 5-100,000 RPM range and a 0.01% accuracy.

EM Heater Design

The dynamometer was useful when measuring the shaft power of the turbine over a range of speeds. A working prototype of the EM-pig heater has a Halbach heating array and not a dynamometer. This section will detail the design of the EM heater.

The heater needed to house the Halbach array and aluminum pipe from the *Experimental Verification* section, and a heat sink to draw the heat from the pipe. The previously tested Halbach array and aluminum pipe had known heating curves that provided certainty when pairing the Halbach array to the turbine set. A heat sink dampened the temperature rise in the aluminum pipe. The heating curves of the Halbach array depend on the conductivity, and therefore the temperature, of the metal pipe.

The EM-heater design consisted of a 5” piece of the 4.25” aluminum pipe held in an acrylic box, see Figure 38. In operation, the acrylic box held water and the Halbach array spun on bearings inside of the aluminum pipe. The box was constructed by laser cutting acrylic sheets to the desired dimensions and using silicon sealant to hold the edges together.

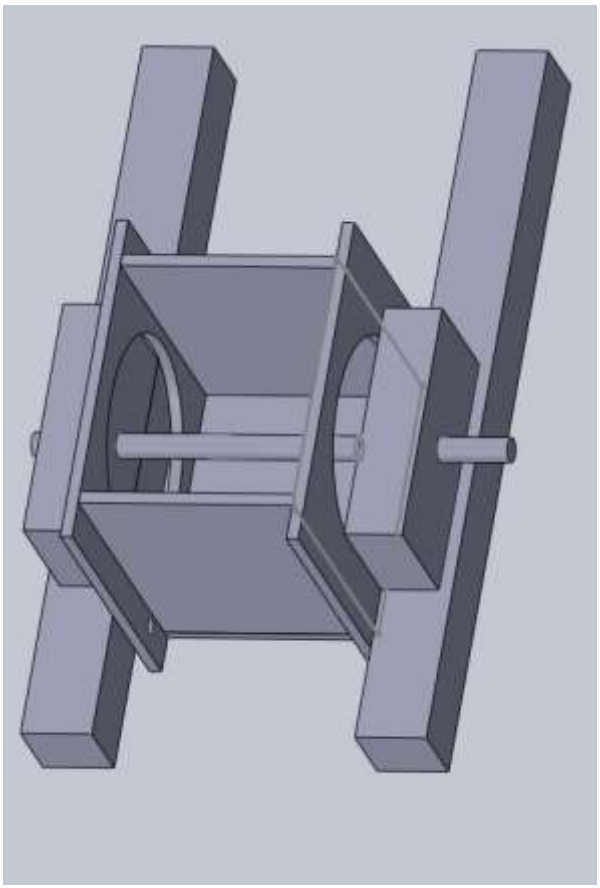

Figure 38. CAD Drawing of EM-Heater without the aluminum pipe.

The final test bed setup can be seen in Figure 39. In Figure 39 the test bed was configured with the dynamometer and testing a turbine which can be viewed in the polycarbonate pipe.

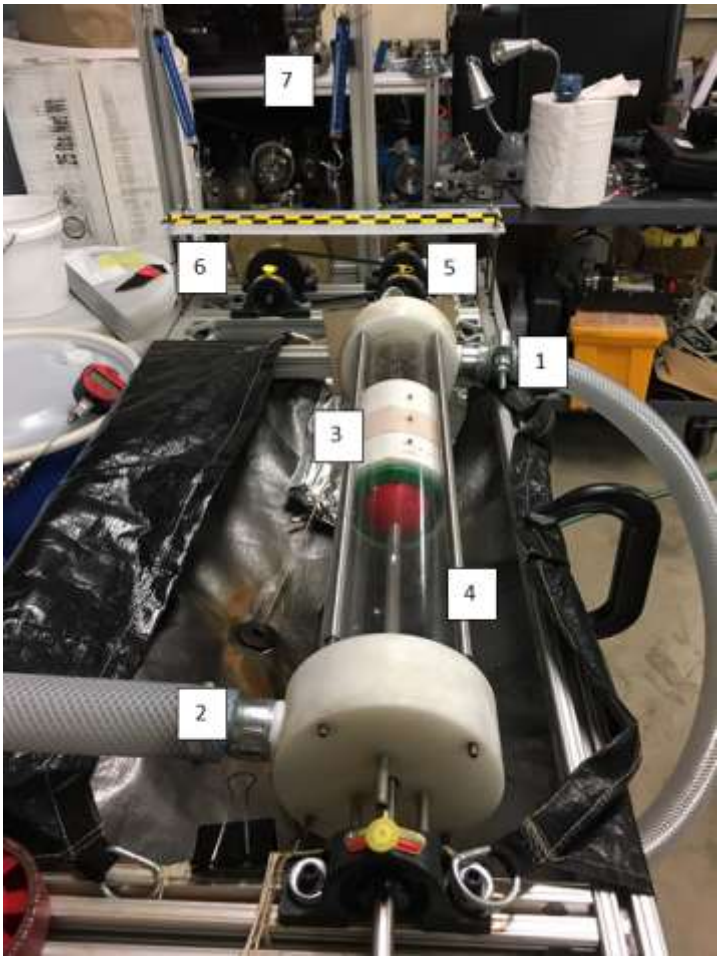

Figure 39. Turbine test bed.

Figure 39 Key:

1- Inlet to test bed
2- Outlet to test bed
3- Multi-stage turbine
4- Test bed with alignment pipes
5- Chain and sprocket for gear reduction
6- Dyno brake wheel
7- Spring scales for torque measurements

Turbine Test Procedure and Test Matrices

The goal of the turbine tests is to:

- Develop a turbine with at least 70% efficiency
- Investigate low n_s propeller type turbines
- Test feasibility of multi-stage turbines
- Test turbine performance under varying flow rates
- Test coupled turbine and EM-heater

This section covers the testing procedures for the turbine test and the test matrices to meet the goals of the turbine tests.

Turbine Test Procedures

This section covers the testing procedures for the turbine dynamometer and EM-heater tests.

Pre-test Check List:

1. Check the water level in the holding tank for fullness.
2. Check wingnuts holding endcaps are secure.
3. Check bearing bolts are tightened properly.
4. Check dynamometer springs are calibrated against each other.
    a. If the test is an EM-Heater test, check if the water level in the EM-heater covers the aluminum pipe. Fill if low.
5. Ensure that drainage hose is draining to a floor drain.
6. Check if hand guard is correctly installed.
7. Don safety glasses.

This checklist was followed in every test.

Turbine Dynamometer Test Procedure:

1. Set spring tension to 1.5lbs and disengage metal band.
2. Turn on the pump.
3. Record turbine speed with a tachometer.
4. Engage metal band.

5. Wait 30 seconds to allow turbine speed to equilibrate.
6. Record both spring scale tensions.
7. Record turbine speed.
8. Record pressure.
9. Increase high tension spring tension by 0.5lbs
10. Check water level and add more if needed.
11. Repeat steps 5-10 until the turbine has stalled. (0 RPM)
12. Test flow rate, see *Flow Indicator*.
13. Shut off the pump.

Turbine EM-Heater Test Procedure

1. Turn on the pump.
2. Wait 30 seconds for speed to equilibrate.
3. Measure and record shaft speed with a tachometer.
4. Test flow rate, see *Flow Indicator*.
5. Change flow rates my operating by-pass valve.
6. Repeat steps 2-5 until the by-pass valve is completely open.
7. Turn off the pump.

Low n_s and Multi-Stage Turbine Test

Low specific speed turbines allow for fewer turbines to be used to generate power. As such, finding the lowest specific speed turbine that would still yield efficiencies of 70% could prove valuable.

The three turbines selected were a 40, 80 and 140 specific speed turbines.

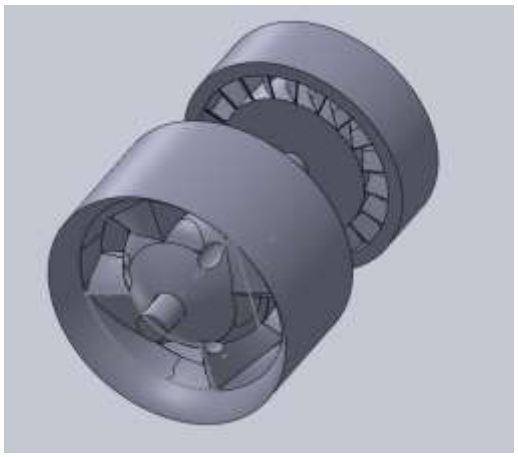

Figure 40. 80 n_s turbine.

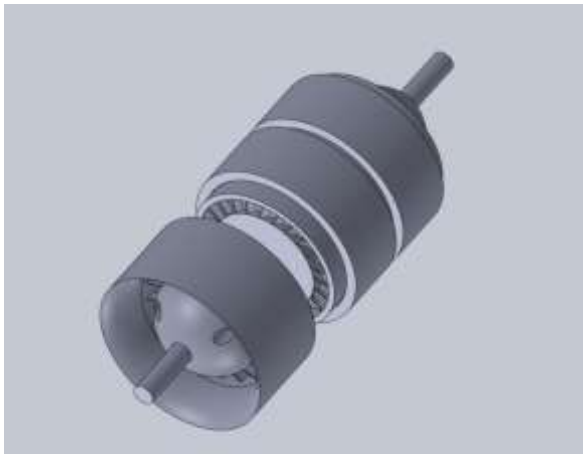

Figure 41. 140 n_s turbine.

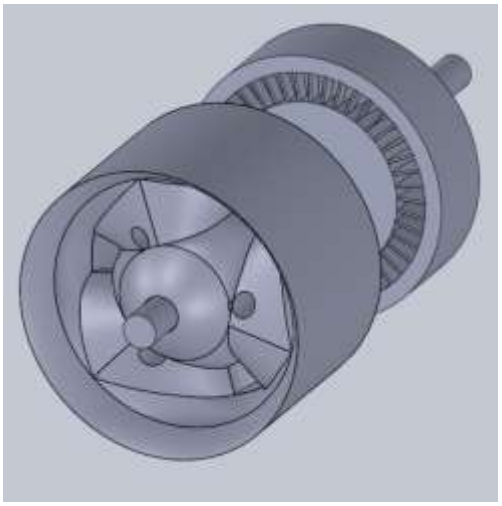

Figure 42. 40 n_s turbine.

Figure 40, Figure 41, and Figure 42 are the SolidWorks models of the three turbines designed with the methodology detailed in *Performance Driven Turbine Design*. The 40 and 80 n_s turbines required nozzling to get high enough flow rates for the blade angles to be reasonable. This nozzling is typical for low specific speed turbines. The 140 n_s turbine required three stages to match the same predicted 160Watt power output of the 40 and 80 n_s turbines. This is an example of how the higher n_s require more stages to achieve the same power output of the lower n_s turbines. Since a multistage turbine was tested during this battery of test, the performance curve of the triple turbine can be compared against the single stage turbines.

Variable Flow Rate Test

The variable flow rate test is required to map the turbine performance under varying flow rates, just at the heater system will experience in the field. The results of the variable flow rate test were used to match the turbine performance to the Halbach array performance for proper gearing ratio, as explained in *Coupled Testing.* The turbine that had the best performance in the varying n_s test, the 140 n_s turbine, was selected for the variable flow rate test. The test was run at 68, 55, 48, and 35GPM flow rates. Lower flow rates could not be tested as 35GPM is the lowest flow rate achievable with our by-pass configuration.

Turbine/EM-Heater Coupled Test

The results of the variable flow rate test produced a comprehensive performance map of the 140n_s turbine. The performance map provided the information for proper gear selection of the turbine and Halbach array. The EM-Heater, and Chain and Sprocket were installed onto the test rig. The chain and sprocket can be seen in Figure 39, item 5. The coupled system was tested under varying flow rates. The operating speeds of the coupled system were compared to the predicted operating speeds, which were found from the performance maps.

Overall Energy Balance of EM-Pig in Operation

The previous sections in the Chapter 3. Methodology discuss the functioning of the heater in the lab. This section takes the EM-heater out of the lab and puts it into the pipeline by providing a conceptual framework to answer the question "How much wax can cause the pig dissolve as it travels down the pipeline?"

We first start with the overall heat balance. The total power required to be generated by the pig is equivalent to the total heat required to dissolve a known volume of wax. This is calculated using equation [23.

$$\dot{Q} = \dot{m} * H_{dil}$$

[23]

Assuming a constant C_p,

If the wax has an average coating of d on the pipe we can replace the mass flow rate of wax on the pig ($\dot{m}$) with $V_{pig} * \rho_{wax} * 2\pi * r * x_{wax}$. We then get:

$$\dot{Q} = V_{pig} * \rho_{wax} * 2\pi * r * x_{wax} * H_{dil}$$

[24]

Where:

r is the pipe radius (m)

V_{pig} is the speed of the pig (m/s)

ρ_{wax} is the wax density (kg/m^3)

x_{wax} is the wax thickness (m)

H_{dil} is the heat of dissolution (J/kg)

To approximate the pressure requirements, we can approximate the power generated by the pig as the enthalpy change in the fluid with an efficiency term.

$$P = (\dot{V} * \Delta P) * \eta$$

[25]

Replacing $\dot{V}$ with $\pi * r^2 * (V_{fluid} - V_{pig})$ where V_{fluid} is the velocity of the working fluid respect to the pipe:

$$P = \pi * r^2 * (V_{fluid} - V_{pig}) * \Delta P * \eta$$

[26]

Setting power generated equal to the heat added:

$$r * \left(V_{fluid} - V_{pig}\right) * \Delta P * \eta = 2 * V_{pig} * \rho_{wax} * x_{wax} * H_{dil}$$

[27]

Or rearranged as we get:

$$x_{wax} = \frac{r * \left(V_{fluid} - V_{pig}\right) * \Delta P * \eta}{2 * V_{pig} * \rho_{wax} * H_{dil}}$$

[28]

Add the term $X_{bypass} = \frac{v_{pipe} - v_{pig}}{v_{pipe}}$, the bypass fraction we get equation [29].

Where:

v_{pipe} is the fluid velocity of the oil in the pipeline (m/s)

v_{pig} is the velocity of the pig down the pipeline (m/s)

$$x_{wax} = \frac{\Delta P * r}{2 * \rho_{wax} * H_{dil}\,(1 - X_{bypass})}$$

[29]

This equation has been graphed in, **Figure 43**.

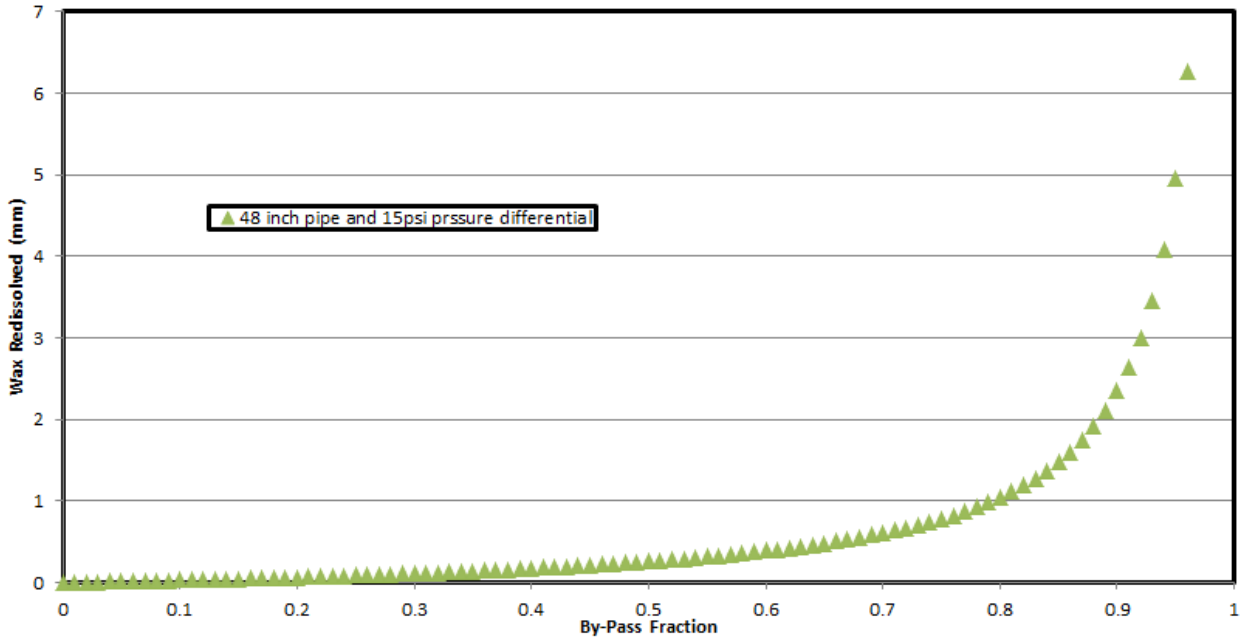

Figure 43. Maximum wax dissolved by pig.

Chapter 4. Results and Discussion

This section presents, interprets and analyzes the results of the testing described in the methodology section.

Halbach Performance

Proper selection of a magnetic array is desired for the self-heating pig design. Correctly sized magnets will convert the shaft power from the magnets into heat at a reasonable rotation speed. Numeric simulations were done, along with experimental work, to characterize the magnet performance. The comparison of these two test sets can be found in the *Comparison* section.

Ansys Simulation Results

Running simulation is advantageous, as it allows a large number of parameters to be evaluated with ease. Fabrication and testing of several Halbach arrays are time and cost intensive, so simulations were carried out to characterize performance. Later sections of the paper discuss the experimental work done to verify the Halbach array performance.

Table 7, which is located in, *Appendix B- Halbach,* and Table 8 show the amount of heat generated per inch of magnets. Heat generation was calculated for each of the parameters determined from the Ansys simulation: pipe diameter, the distance between magnets and wall (air gap), the speed of magnet array, wall thickness, and wall material.

The results of the Ansys simulation are found in Table 7 located in *Appendix B- Halbach*.

A relationship for the heat generated as a function of speed and diameter can be found using regression. The results of the regression with varying wall thickness and air gap are shown in Table 4. The results are shown with values of *a, b,* and *c,* which correlate to the values seen in equation [30.

$$\frac{Heat\ (W)}{inch\ of\ magnet} = a * \omega\ (RPM)^b * Diameter\ (in)^c$$

[30]

Table 4. Power regression results of Ansys simulation.

Air Gap (in)	0.05	0.025	0.1	0.05	0.05	0.05
Thickness (in)	0.25	0.25	0.25	0.125	0.375	0.25
Metal	Steel	Steel	Steel	Steel	Steel	Aluminum
"a"	6.03E-06	8.69E-06	2.93E-06	5.29E-06	6.01E-06	4.95E-05
"b"	1.8593	1.8593	1.8593	1.8593	1.8593	1.8593
"c"	2.9265	2.9265	2.9265	2.9265	2.9265	2.9265
R^2	0.9997	0.9997	0.9997	0.9997	0.9997	0.9997

The high R^2 from the regression indicate that the power regression is adequate to express the heat generation for this variable space. Based on the results, aluminum (how about brass which is more corrosion resistant) appears to have the greatest impact on the heat generated, see *Appendix B- Halbach*. This is due to its relatively high electrical conductivity relative to steel. The values of "b" and "c" were not recalculated for each point but rather were calculated once using the sensitivity analysis of magnet speed and diameter.

Experimental Results

An experiment was conducted to compare against the Ansys simulation and gain accurate data to characterize the magnet performance. The accurate magnet performance was required to properly gear the magnet array to the turbine.

The results of the Halbach experimental test are shown in Figure 44.

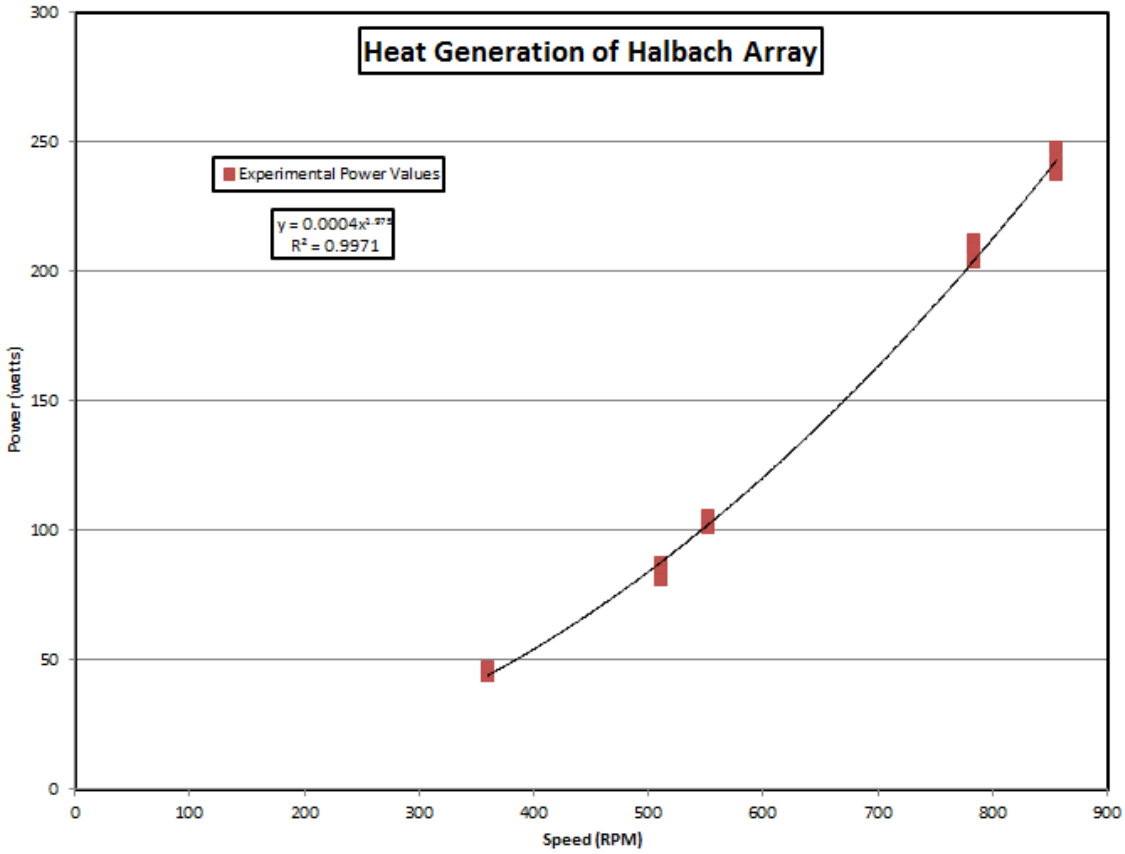

Figure 44. Halbach array heating results.

The power exponent for speed obtained for this test is 1.975, as seen in Figure 44, and the "a" , from equation [30] value is $6.12 * 10^{-6} \frac{\frac{W}{in}}{\omega^{b} * D^{c}}$.

Comparison

This section will compare the "a" and "b" values between the Ansys simulation and the experimental work. The "c" values will not be compared as there was no work done in the experimental to vary the magnet array diameter.

Comparing "a" values

The experimental results were done using an aluminum pipe of 0.125 inches thick with an air gap of 0.1in. However, no simulations were conducted using those particular parameters. Using assumptions that the effects of air gap and pipe thickness are independent of each other and the material used, the expected "a" value is $1.90 * 10^{-5} \frac{\frac{W}{in}}{\omega^{b} * D^{c}}$. This was done by using the

simulation “a” value for an aluminum pipe at 0.125in and applying the same relative change seen in the air gap sensitivity test. The experimental value of $6.12 * 10^{-6} \frac{\frac{W}{in}}{\omega^b * D^c}$ is 3.09 times smaller than the expected value.

There are a variety of factors that could explain this discrepancy. The conductivity of the material can significantly affect the “a” value. The conductivity of the aluminum pipe was not verified against the values used in the simulation. Heat loss to the environment would decrease the observed heating and the value of “a.” The initial assumption that the effect of the air gap is independent of other parameters may not be correct. If the air gap effect is not independent of the material or pipe wall thickness, then the expected “a” value of $1.90 * 10^{-5} \frac{\frac{W}{in}}{\omega^b * D^c}$ from the modeling may not be correct.

Comparing “b” values

The “b” value or the power relationship of magnet speed, see Equation [30, was observed as 1.975 while the Ansys simulation predicted a value of 1.859. This puts the relative error at 5.8% which is well within the expected experimental variability.

Turbine Performance

When installed into a pig, the Halbach arrays will be driven by a turbine, or series of turbines, through a pre-selected gear ratio. The gear ratio will be selected to allow the turbines to turn the magnets at speeds which the turbines produce the maximum power. This section presents the turbine performance curves needed to select the proper gear ratio for the Halbach array. This section also looks at effects of low specific speed and stacking turbines in series on the overall efficiency of the turbine. These results will be used to optimize the turbine performance.

Effect of Specific Speed on Performance and Efficiency

The specific speed of a turbine is a number characterizing how many revolutions of a turbine are needed to do a particular amount of work. A turbine that can operate at a low

specific speed, or more power per turn, could power the magnets at a lower gear ratio and use fewer turbines. This section investigated the effect of high and low specific speed on the overall performance and efficiency of the turbines.

Comparison between Designs of Varying N_{sp}

Fixed propeller type axial turbines are known to operate most efficiently at specific speeds of one hundred to two hundred. The tests done below are on three turbines of varying specific speeds of 40, 80, and 140. The 40 and 80 specific speed turbines used nozzled flow, while the 140 specific speed turbines used three turbines in series to achieve the similar overall pressure drops to the 40 and 80. The tests, completed in Figure 45 were conducted at flow rates between 68 and 73 gallons per minute.

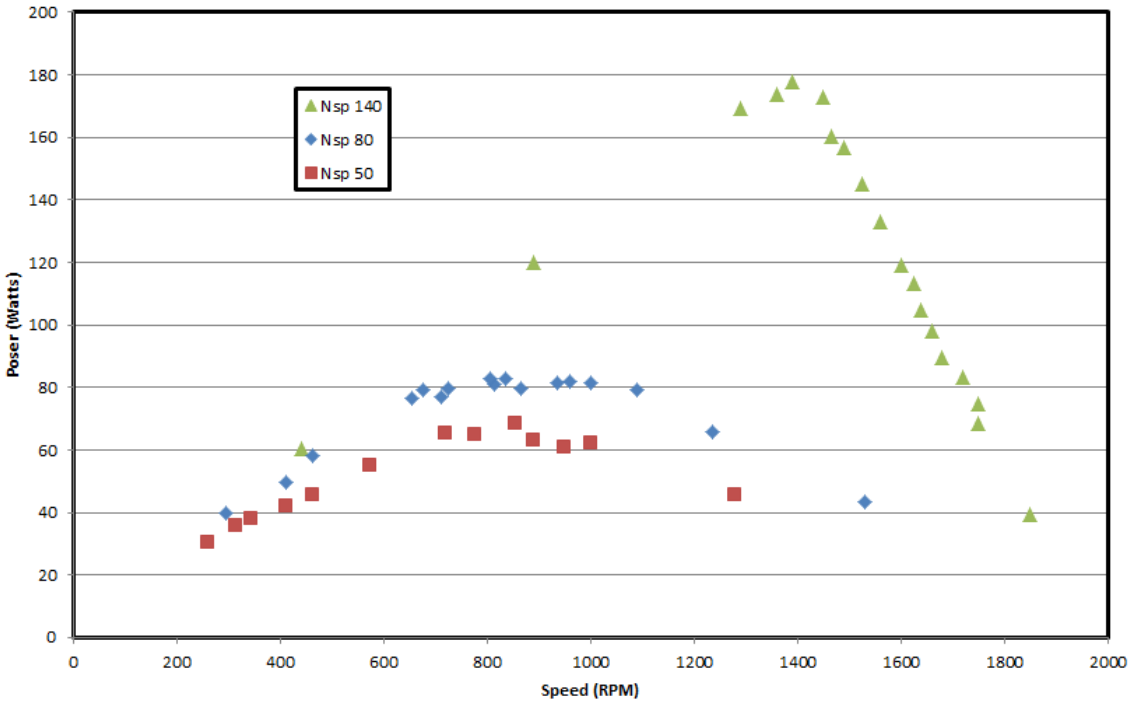

Figure 45. Turbine Performance Curves at Varying Specific Speeds.

As expected, the higher specific speed turbines had peak power at higher speeds. What is not shown is the expected speed at which maximum power is achieved versus the experimental values, these are found in Table 5.

Table 5. Performance Benchmarks of Varying Specific Speed Turbines.

	Speed at Max Power (RPM)		Max Power (Watts)		
Nsp	Expected	Actual	Expected	Actual	Efficiency
140	1400	1390	160	177	0.78
80	600	1000	160	82	0.37
40	450	855	160	68	0.27

As seen in Table 5, the higher specific speed turbine has more predictable performance, higher power output, and greater efficiency than the lower specific speed turbines.

Correcting for Orifice Pressure Drop

The lower efficiencies of the of the 80 and 40 specific speed turbines can be partially accounted for using the equations used to describe orifice flow, which are derivative from Bernoulli's equation. Equation 31 is a derivative of Bernoulli's equation that relates flow through an orifice and the pressure drop across it.

$$q_v = A_{orifice} * \sqrt{\frac{2 * \Delta p}{\rho * \left(1 - \left(\frac{d_{orifice}}{d_{pipe}}\right)^4\right)}} \quad [31]$$

$$\Delta p = \frac{\left(q_v^2 * \rho * \left(1 - \left(\frac{d_{orifice}}{d_{pipe}}\right)^4\right)\right)}{\left(2 * A_{orifice}^2\right)} \quad [32]$$

Using the values of the nozzle areas on the 40 and 80 specific speed turbines, the pressure drop contributions of the nozzling are 4.2 and 3.5 psi, respectively. To gauge the effect of the nozzled flow on the total efficiency, the efficiencies were recalculated using pressure drop calculated using equation [32] that ignored the contributions due to the nozzled flow.

Table 6. Efficiencies without Orifice Effect.

	Efficiency	
Nsp	Real	Without Orifice ΔP
140	0.78	0.84
80	0.37	0.64
40	0.27	0.62

Ignoring the pressure drop from the nozzling, the efficiencies of the 80 and 40 specific speed turbines do increase significantly but still are still lower than the 140 specific speed turbine. At higher flow rates where nozzling may not be required to achieve lower specific speeds, the low specific speed turbines may be feasible for a turbine design. However, the conventional knowledge that fixed propeller type turbines operate well in specific speeds between 100 and 200 still seems to hold and, if practical, should be practiced.

Performance Curves under Varying Speed and Flow Rate

The performance curves of a particular turbine will vary as a function of flow rate. The same turbine with more fluid moving through it could be expected to produce more power and at a higher speed. A turbine/magnet pairing that was selected for a particular flow rate may not perform well under differing flow rates. Understanding how the performance of a turbine varies under varying flow rates allows for the calculation of an optimal operating window for a turbine/magnet pairing. Ultimately, this operating window dictates what range of pigging speeds and pipelines of varying flow rates the EM-pig will be able to efficiently pig.

Test Results

The triple turbine performance curves were tested from flow rates ranging from 35 to 68 gallons per minute. The results can be seen in Figure 46.

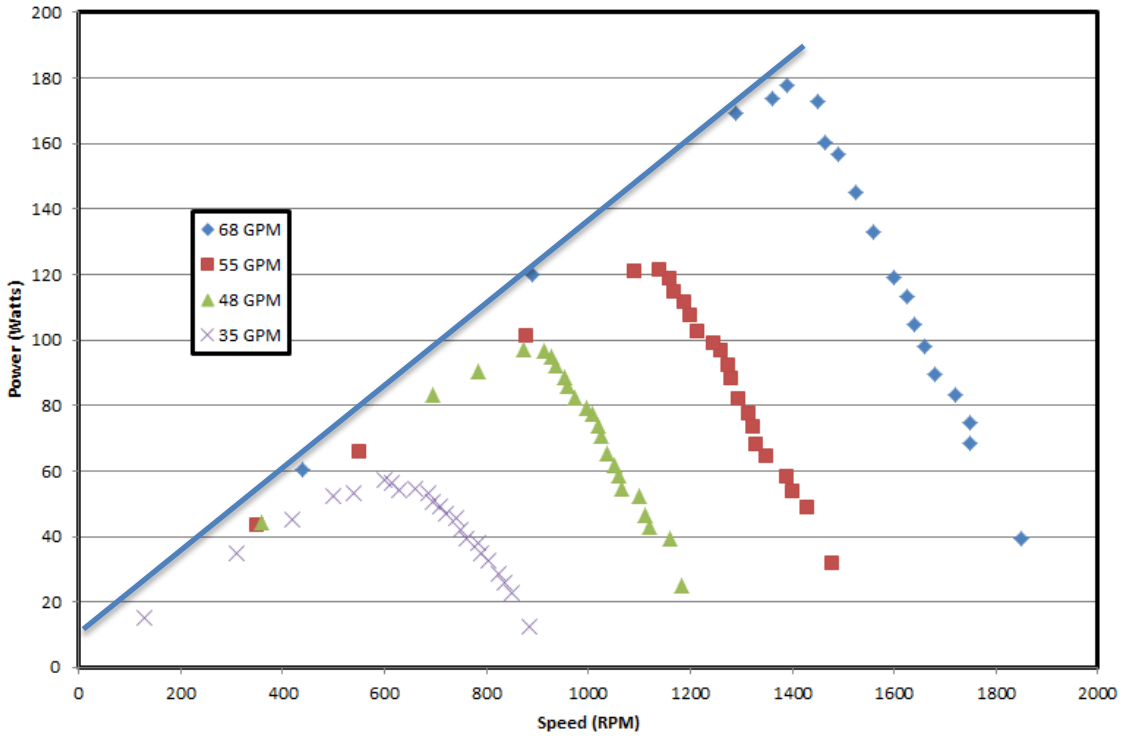

Figure 46 Performance Curves at Varying Flow Rates

The maximum power generated by the turbines appears to be proportional to the flow rate to the 1.77 power. (See *Appendix C- Turbine Tests*)

$$P \propto Q^{1.77}$$

[33]

This is close to the predicted square relationship between power and flow rate. The small sample size and error associated with the measurements could account for the discrepancy between the observed and predicted power/flow rate relationship.

Another potential cause of a lower than expected power relationship could be due to artificially low power readings at higher flow rates. The 48, 55, and 68 GPM test power values seem to be linear at lower RPM values, see Figure 46. This indicates that the observed torque readings did not change much at these low speeds, see Figure 47. This flat-lining of the torque is not present on the lowest flow rate test, see Figure 46, or on the 80 or 40 specific speed turbine tests, see Figure 45. These tests produced less torque than the high flow rate 140 specific speed

turbines, see Figure 47. It is possible that this flat lining of torque values is an artifact of the torque wheel rather than the turbines.

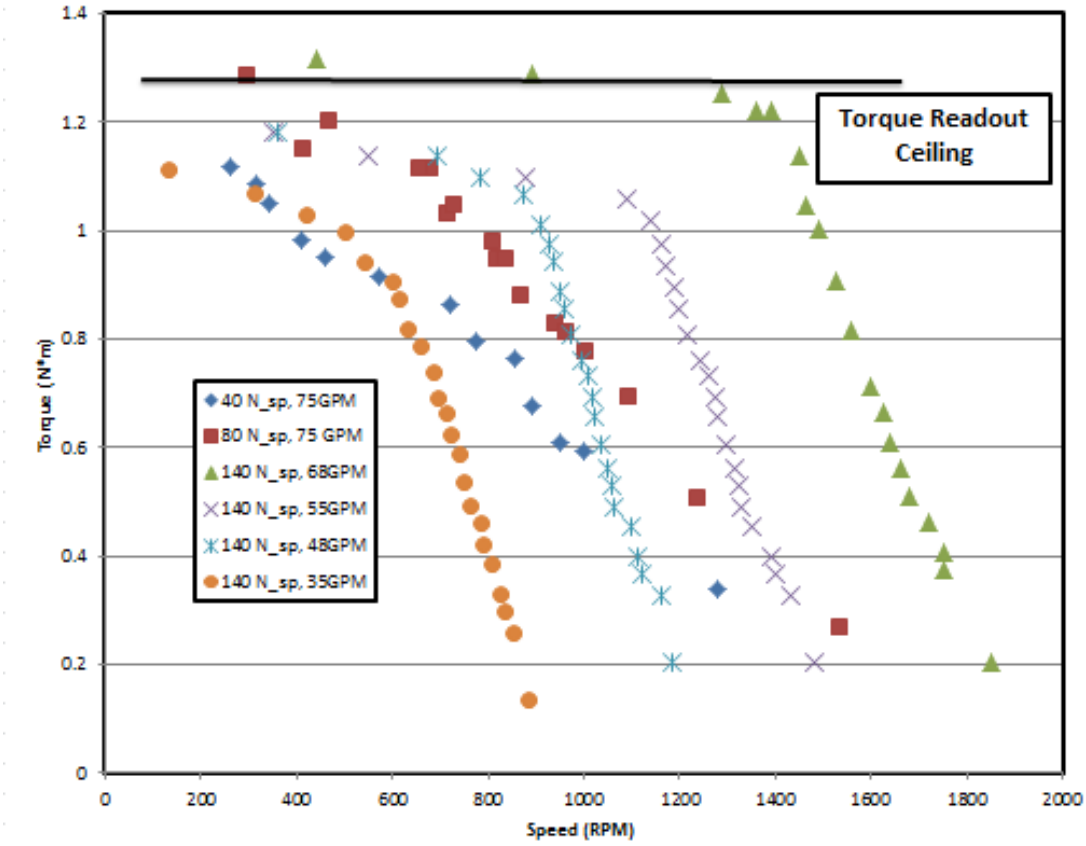

Figure 47 Torque Curves of Various Turbines

Effect of Multi-Stage Turbine

If an error in the reading equipment is not the cause of the torque flat lining, the turbine design could be the cause. The 140 specific speed turbine, used in the tests above, was a three-stage turbine.

The set of turbines are designed to operate at a specific flow rate and rotational speed. As the working fluid leaves stage *n* rotor at angle θ and enters the stator at stage *n+1* which has an angle of θ, this angle is by design. If the speed is changed, then the angle the working fluid changes to *(ϑ+δ).* Now the working fluid, with an angle of *(ϑ+δ),* enters the stator with an angle of θ. This incongruence between the direction of flow entering the stator and the direction of the stator blades could lead to a loss of performance in the turbine. The multistage turbines

appear to perform well at and above the design speed but not below the design speed. The loss of performance at non-design speeds could be due to the incompatibility of the fluid and blade angles.

Operating Window Movement and Comparison to Magnet Performance

Since the pig will be operating under varying flow rates, the magnet/turbine pairing will need to be functional under varying flow rates. A set of turbines and magnets can be geared to the proper gear ratio for a particular flow rate. Figure 48 shows results for pairing the 140 specific speed turbine with the magnet array tested previously. A gear ratio of 1:2, one revolution of the magnets for every two revolutions of the turbine, was selected as it allowed the turbine and magnets to operate near the maximum power of the turbine. The pairing should operate at near the intersection of the two curves as this is the point at which the power required to spin the Halbach array at a speed is the power supplied by the turbine.

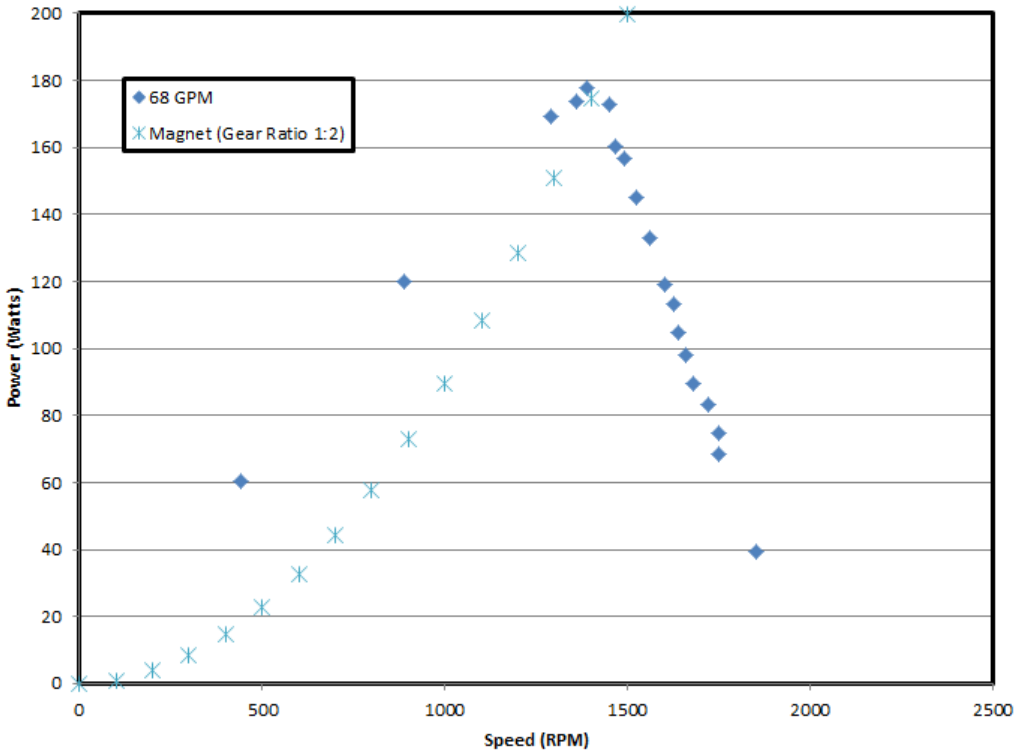

Figure 48. Magnet and Turbine Pairing for 68GPM.

This 1:2 gear ratio works well for the 68GPM flow rate, but the pairing does not hit peak power for the lower flow rates, see Figure 49. At 35GPM the 1:2 gear ratio would result in a

power output of 48 Watts, which is 17% lower than the maximum power that the turbine could provide at that flow rate, see Figure 49.

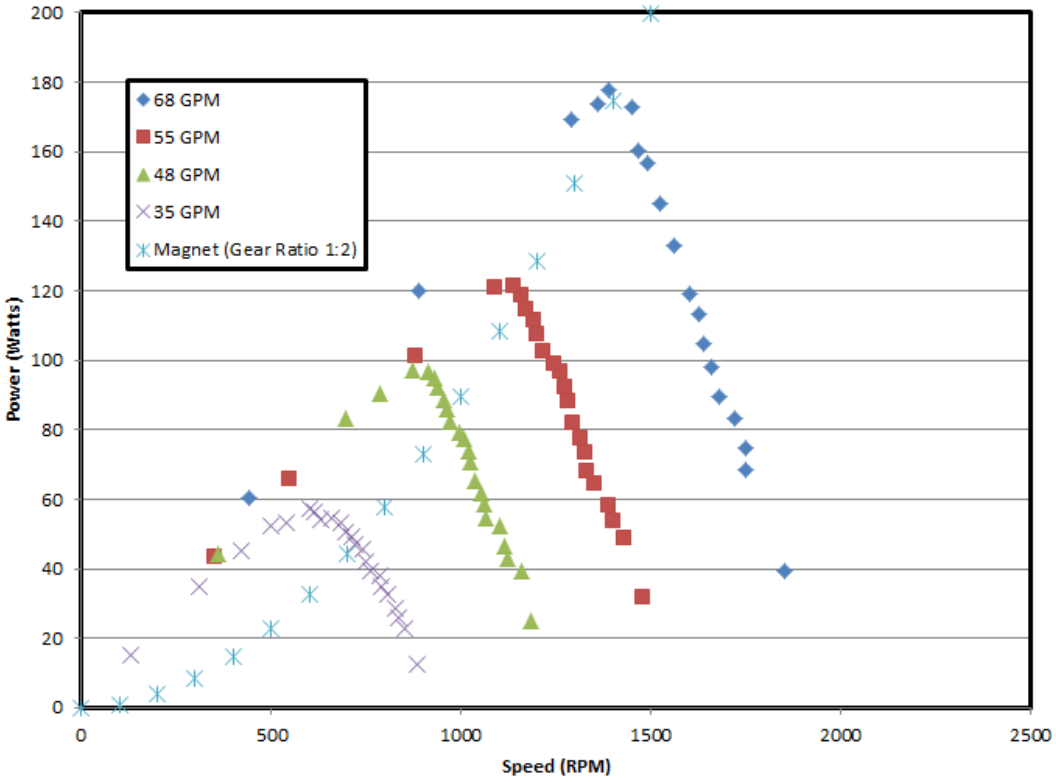

Figure 49. Magnet/Turbine Performance For Varying Flow Rates.

This is evident as the power/speed relationship for the Halbach array was observed at:

$$P_{Halbach} \propto \omega^{1.98} \quad \textbf{[34]}$$

Whereas the relationship between the max produced power by the turbines and speed is:

$$P_{max} \propto \omega^{1.36} \quad \textbf{[35]}$$

(See Figure 55 in *Appendix C- Turbine Tests*)

Since the $P_{Halbach}$ and P_{max} relationships to speed do not follow the same power, they cannot align over all speeds. This means the gear ratio for a particular Halbach array and turbine

will need to be chosen to optimize the power output for a particular flow rate and speed. In practice the gear ratio should be selected to maximize power when it will be needed the most, such as at low pigging speeds when there would the greatest heat demand. The sacrifices at lower flow rates are not particularly high as the lab tests done show that a paired magnet and turbine array only lose 17% of the maximum power when the flow rate is about half what the gear ratio was selected for.

Turbine-Magnet Coupled Performance

In a final test to develop a working prototype of the turbine heater, the brake wheel was removed and replaced by a Halbach array, with a 1:2 gear ratio. The predicted performance for each flow rate is where the Halbach and turbine curves intersect in Figure 49. The anticipated performance was compared to the observed performance in Figure 50.

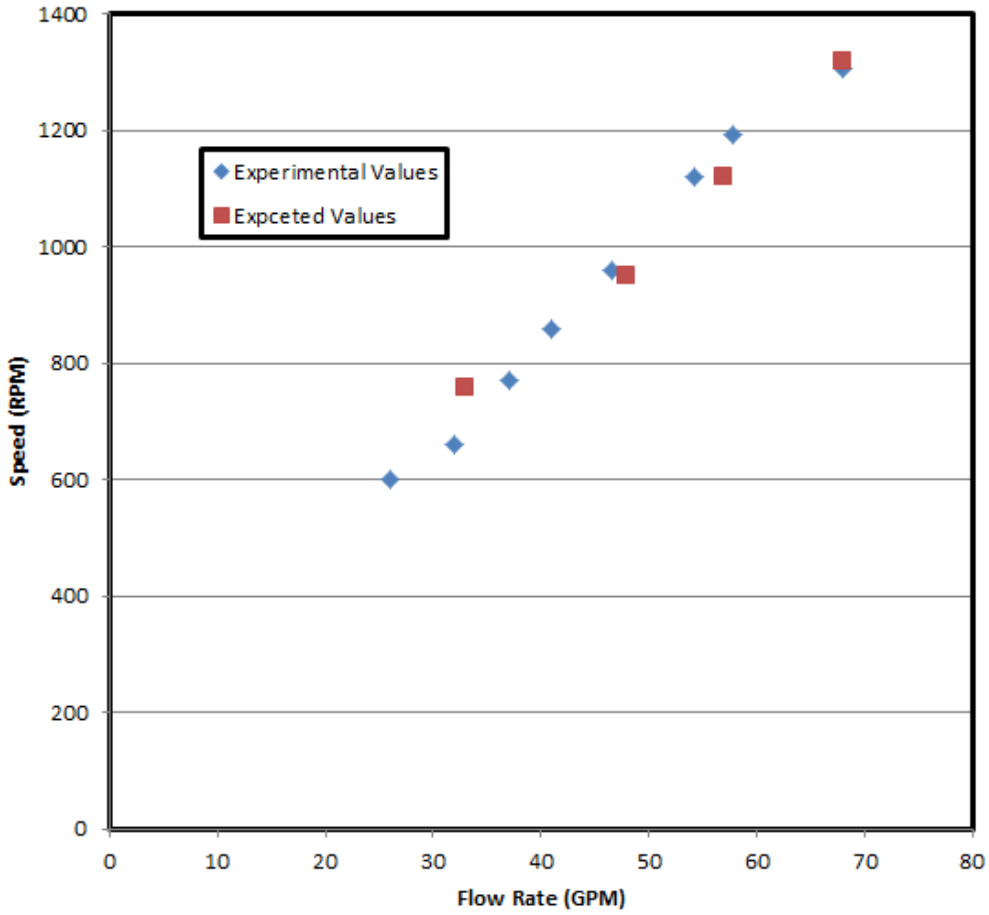

Figure 50. Predicted and Observed Coupled Turbine/Magnet Performance.

The predicted and observed performances of this coupled system are considerably very close with an average error of less than 2% between the two. This low error is expected as the expected performance was determined through experimental results from the turbines and Halbach array used. The low error indicated the overall error in turbine power test and magnet power tests were low.

Chapter 5. Conclusions

Based in the simulations and experiments conducted, the following conclusions are made.

- Analytical methods can produce turbines with relatively high efficiency and with predictable performance. In this study, an analytical approach to the design created a turbine geometry that tested at 78% efficiency and peak power at the predicted RPM. Predictable peak power at the expected RPM allows for less, or no, performance testing for Halbach gear matching. This could prove valuable when scaling to field testing.
- Ansys modeling was able to properly predict the relationship between magnet speed and heat dissipated. However, the Ansys modeling was not able to predict the heat dissipation at a particular speed. This inaccuracy may be accounted by an error in material properties used rather than an error in the model.
- Further work on Halbach performance at elevated temperatures should be done when designing the pig as elevated temperatures change the conductivity of the metals and the magnetic field strength.
- Propeller turbines perform well at specific speeds above 100. Lower specific speed turbines may seem attractive for the reduced number of stages and easier gearing ratio but will come at the expense of efficiency.
- Based on the lab tests, a single gear ratio can match a turbine and Halbach array over a several fold variance in flow rate. This indicates that a single self-heating pig design would be operable in pipelines with varying flow rates and when the pig is operating over varying by-pass ratios.
- Building a self-heating pig that can melt wax is very possible, though it would need to travel down the pipe slowly. The overall heat balance shows that for a pig like this to melt a considerable amount of wax under reasonable conditions, the pig would need to travel at or below 15% of the overall fluid velocity. Controlling for pig speed could be achieved through proper turbine selection and use of a properly sized orifice as detailed in *Optimizing Flow Assurance Using Pigging in Sub-Sea Pipelines* (Wit, 2015). Dynamic control could be achieved through an adjustable choke.

Chapter 6. Appendix

Appendix A- Methodology

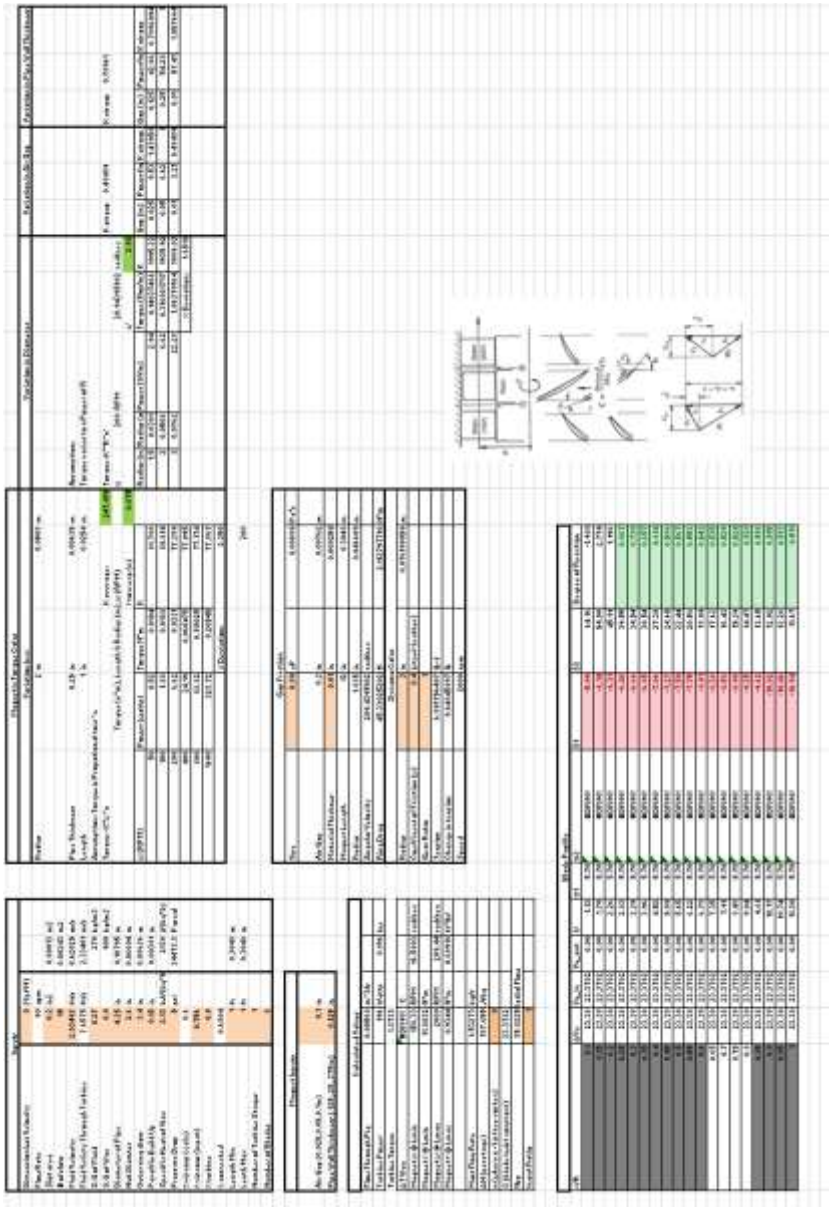

Figure 51. Screenshot of Blade Geometry Spreadsheet.

Appendix B- Halbach

Table 7. Ansys Simulation with varying pipe diameter and speed.

Pipe Diameter (in)	6	3	4	4	4	4	4	4
Air Gap (in)	0.05	0.05	0.05	0.05	0.05	0.05	0.05	0.05
Angular Velocity (RPM)	200	200	50	100	200	400	800	1600
Pipe Wall Thickness (in)	0.25	0.25	0.25	0.25	0.25	0.25	0.25	0.25
Metal	Steel	Steel	Steel	Steel	Steel	Steel	Steel	Steel
Power Loss (w/in)	22.28	2.94	0.52	1.88	6.62	24.19	88.82	328.72`

Table 8. Ansys Simulation with varying air gap, pipe wall thickness, and pipe wall material.

Pipe Diameter (in)	4	4	4	4	4	4	4
Air Gap (in)	0.025	0.1	0.05	0.05	0.05	0.05	0.05
Angular Velocity (RPM)	200	200	200	200	200	200	200
Pipe Wall Thickness (in)	0.25	0.25	0.125	0.25	0.375	0.25	0.25
Metal	Steel	Steel	Steel	Steel	Steel	Steel	Aluminum
Power Loss (w/in)	9.53	3.21	5.8	6.62	6.59	6.62	54.28

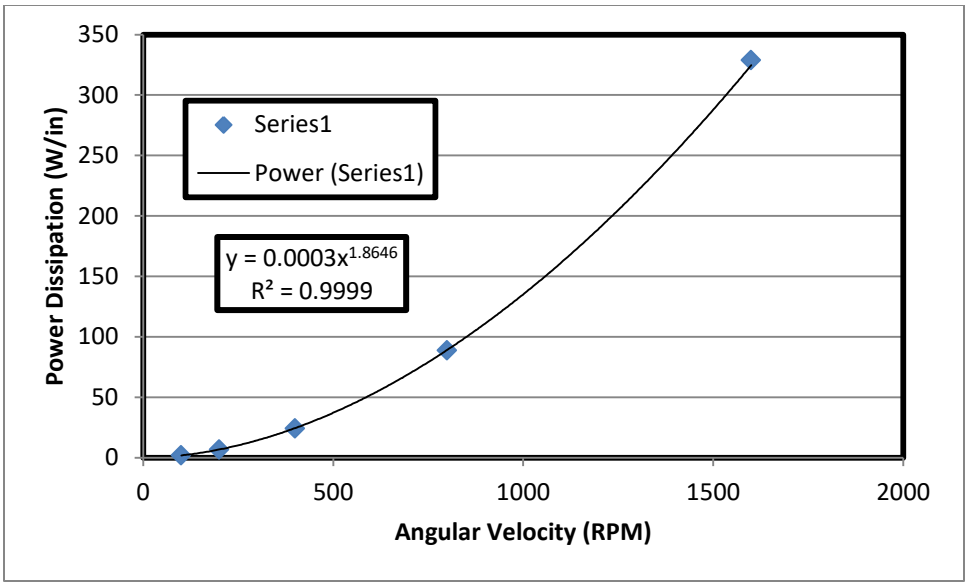

Figure 52. Power regression of speed sensitivity test.

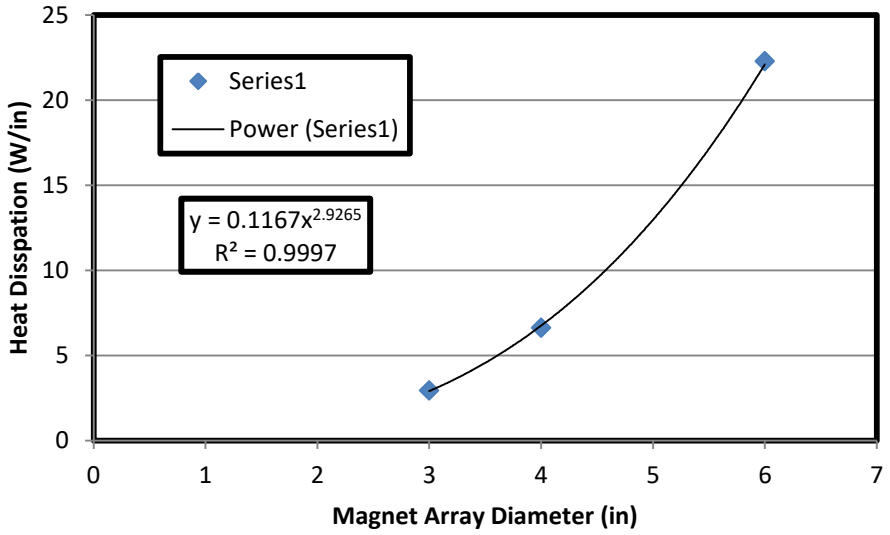

Figure 53. Power regression of diameter sensitivity test.

Appendix C- Turbine Tests

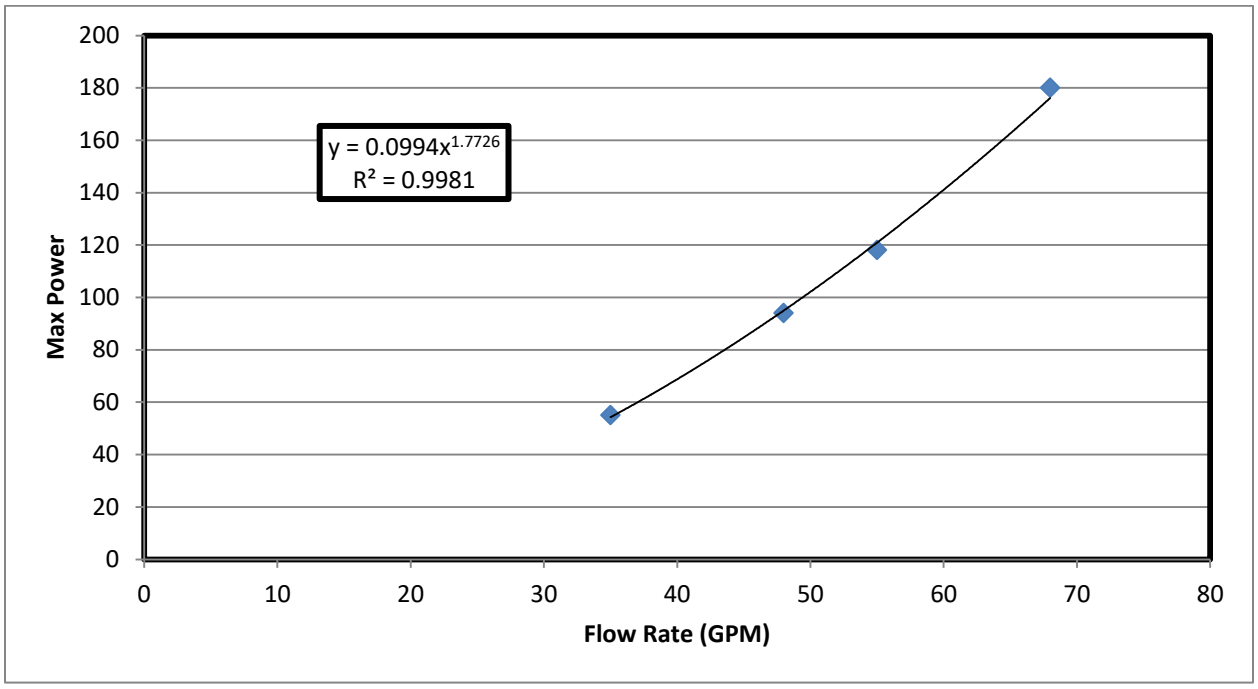

Figure 54. Maximum Power with Varying Flow Rates.

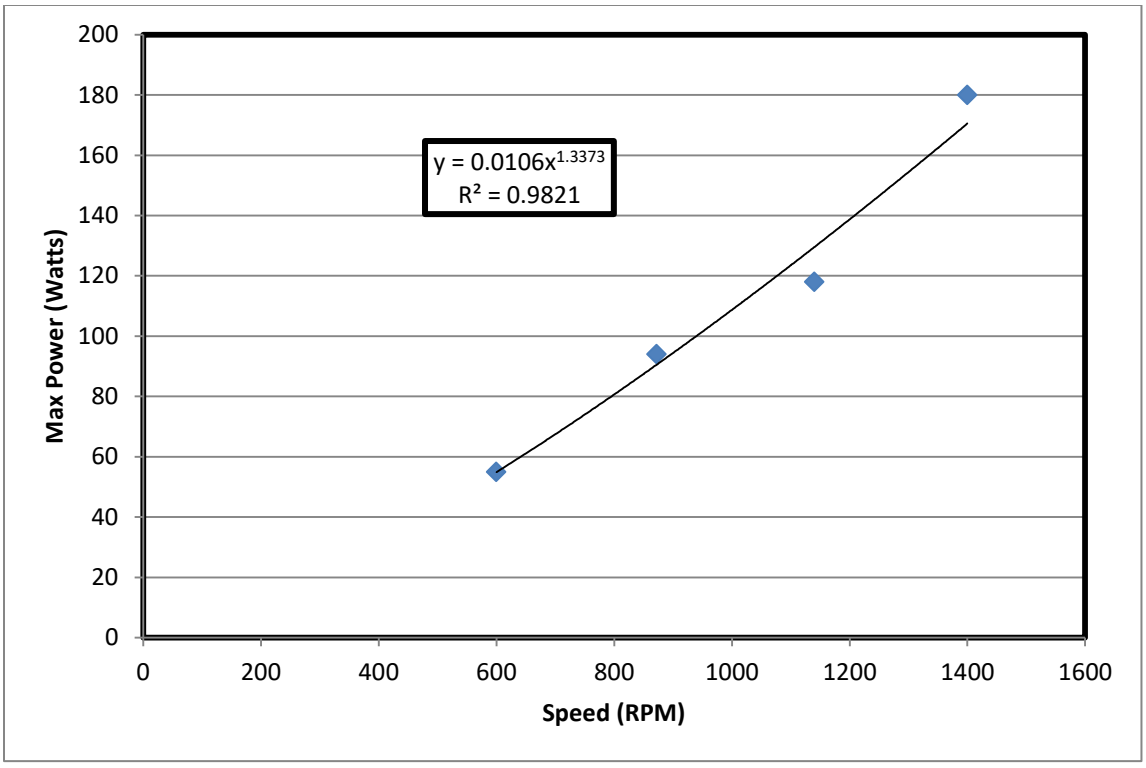

Figure 55. Max Power Observed Relationship to Speed in N_{sp} 140 Turbine.

References

Al-Yaari, M. (2011, January 1). Paraffin Wax Deposition: Mitigation and Removal Techniques. Society of Petroleum Engineers. doi:10.2118/155412-MS

Bagdat, Mombekov, and Rashidi Masoud. "Control of Paraffin Deposition in Production Operation by Using Ethylene–TetraFluoroEthylene (ETFE)." *Springer Science+Business Media Singapore* (2015): 13-21. Print.

Bailey, Alan. "The Headache of Low Oil Flow in TAPS." *The Headache of Low Oil Flow in TAPS - February 07, 2016 - Petroleum News*. Petroleum News, 07 Feb. 2016. Web. 09 June 2017.

Blumler, Peter, and Frederico Casanova. "Hardware Developments: Halbach Arrays." (2016): 133-54. Print.

Courton, Chris, and Lucus Stern. "Eddy Currents." *Joseph Henry Project*. Princeton University, 26 Mar. 2016. Web. 6 June 2017

Dobbs, James B. "A Unique Method of Paraffin Control in Production Operation," SPE 55647, Unichem, A division of BJ Services Company, Presented at the 1999 SPE Rocky Mountain Regional Meeting

Duramag. "Benefits and Drawbacks of Using Halbach Arrays." *Duramag*. N.p., 12 May 2016. Web. 6 June 2017.

Dwyer Instruments. *Dwyer DPGA-06 Pressure Gauge*. Digital image. *Alliedelec*. Alliedelec, n.d. Web. 1 June 2017.

Fung, G., Backhaus, W. P., McDaniel, S., & Erdogmus, M. (2006, January 1). To Pig or Not to Pig: The Marlin Experience With Stuck Pig. Offshore Technology Conference. doi:10.4043/18387-MS

Gupta, A., & Anirbid, S. (2015). Need of Flow Assurance for Crude Oil Pipelines: A Review. *International Journal of Multidisciplinary Sciences and Engineering*, *6*(2), 1-7.

Haimbaugh, Richard E. *Practical Induction Heat Treating*. Materials Park, OH: ASM International, 2001. Print.

Hashem, Dr. Abdel-Alem. "Oil and Gas Pipeline Design, Maintenance and Repair." 22 Mar. 2016. Lecture.

Jordan, Edward; Balmain, Keith G. (1968). *Electromagnetic Waves and Radiating Systems* (2nd ed.). Prentice-Hall. p. 100

K&Y Magnets. *Temperature and Neodymium Magnets*. N.p., June 2014. Web. 07 June 2017.

Merritt, Bernard, and Robert Post. "Halbach Generators and Motors." *Halbach Array Motor/Generators* (n.d.): 1-8. *HCKM*. 3 Feb. 1995. Web. 6 June 2017..

Seredyuk, V and M. Psyuk, "The Method for Increasing the Efficiency of Asphalt-Resin-Paraffin Deposits Inhibitors," 2009, pp. 313-317

Smith, David R., Jerome G. Hust, and Lambrt J. Van Poolen. "Effective Thermal Conductivity of a Glass Fiberglass Blanket Standard Reference Material." (1981): n. pag. Print.

Southern California Gas Company. "IN-LINE INSPECTION OF PIPELINES." (2013): 1-2. Southern California Gas Company, Jan. 2013. Web. 22 Mar. 2016.

Todi, S., & Deo, M. (2006, January 1). Experimental and Modeling Studies of Wax Deposition in Crude-Oil-Carrying Pipelines. Offshore Technology Conference. doi:10.4043/18368-MS

Turton, Robert Keith. *Principles of Turbomachinery*. London: Chapman & Hall, 1995. Print.

US DOT. "Pipeline Safety Stakeholder Communications." *PHMSA: Stakeholder Communications - Smart Pig Fact Sheet*. US DOT, 2014. Web. 08 June 2017.

Waldman, Jonathan. *Rust: The Longest War*. New York: Simon & Schuster Paperbacks, 2016. Print.

White, Frank. *Fluid Mechanics Seventh Edition*. 7th ed. New York City: McGraw-Hill, 2011. Print.

Wit, Derek de. *Optimizing Flow Assurance Using Pigging in Sub-Sea Pipelines*. Diss. U of Witwatersrand, 2015. N.p.: n.p., n.d. Print.